DEVELOPMENT OF METAL-BASED RADIOPHARMACEUTICALS FOR POSITRON EMISSION TOMOGRAPHY IMAGING: PRODUCTION OF ZINC-63 AND MOLECULAR DESIGN FOR GALLIUM-68 LABELED PROBES

by

Guerra Gómez Francisco Lázaro

Chiba, Japan

February 2013

要旨

論文題名

ポジトロン断層法イメージングに使用する金属放射性薬剤の開発について：亜鉛 63 の製造とガリウム標識プローブの分子設計

[背景] ポジトロン断層法「PET」は、陽電子放出核種から放出された陽電子と陰電子とが衝突して生成する 2 個の消滅ガンマ線を対向に設置された検出器で同時に検出することにより，優れた解像度と高い感度および定量性を併せ持つ分子イメージング技術である。PET では陽電子放出核種で標識された薬剤（プローブ）を人体に投与し、目的組織に集積したプローブから発生された消滅ガンマ線を検出することにより、分子・細胞レベルにおける生物学的なプロセスを in vivo で可視化、計測する。亜鉛は生体関連プロセスに関わる必須金属であり、その陽電子放出核種は、亜鉛の生体内プロセスを直接評価できるため、高い関心を集めている。しかし、利用可能な放射性亜鉛には ^{62}Zn と ^{65}Zn があるが、これらの放射性核種は分子イメージングで最適な性質を有していない。一方、ゲルマニウム/ガリウムジェネレータから溶出可能なガリウム-68「^{68}Ga」はサイクロトロンを必要としない陽電子放出核種として関心を集めている。^{68}Ga では標的分子認識素子を持つ放射性プローブを調整するために様々な二官能性キレートが開発されている。その一つに、分子内に複数分子の標的分子認識素子を導入可能な 1,4,7-triazacyclononane -1,4,7-tris-(glutaric acid) (NOTGA)がある。NOTGA にはジアステレオマーを含む構造異性体が生成するが、これまでにそれらの詳細な評価は行われていない。そこで、本研究では分子イメージングに適した性質を持つ ^{63}Zn の新たな製造および精製システムの開発と、多量体ガリウム放射性薬剤用の 1,4,7-triazacyclononane -1,4,7-tris-(glutaric acid) (NOTGA)ジアステレオマーの合成およびそれらの評価を行った。

陽電子を放出する亜鉛 63 の製造に関する基礎的研究

「背景」陽電子を放出する亜鉛には亜鉛 62「^{62}Zn」、亜鉛 63「^{63}Zn」および亜鉛 65「^{65}Zn」がある。^{62}Zn は半減期 9.3 h で陽電子放出核種である ^{62}Cu「$T_{1/2}$ = 9.7 min」に壊変し、また ^{65}Zn は 243.9 日と非常に長い半減期を有する。一方、^{63}Zn は半減期 38.5 分で、安定同位体 ^{63}Cu に壊変することから、^{63}Zn は核医学イメージングにおいてより望ましい性質を有する。これまでの ^{62}Zn および ^{65}Zn を用いた報告から ^{63}Zn は腫瘍またはすい臓疾患のイメージングに有用と考えられる。

「方法と結果」天然由来銅ターゲット「^{63}Cu: 69.17% ・^{65}Cu: 30.83%」に 13.5 MeV の陽子を照射し、^{63}Zn を製造した。その後、陽イオン交換カラム「0.05 N HCl-85%アセトン」により精製し総収率 169 ± 30 MBq/μA·h で ^{63}Zn を得た。放射化学的純度は 99%以上で、不純物として ^{65}Zn のみ観察された。一方、照射 1.6 時間後の比放射能は 29.4 GBq/μmol であった。ターゲットである Cu の残存量は 0.04 μg/g 以下であった。ラットを用いた PET 撮像では ^{63}Zn の体内動態は以前報告された ^{65}Zn の動態と一致し、すい臓に高い集積を示し、^{63}Zn の分子イメージングへの応用の可能性が認められた。

「考察」^{63}Zn の製造および精製法を確立した。その方法は迅速かつ直接的であり高い化学的および放射科学的純度で ^{63}Zn を得た。PET 画像において亜鉛のすい臓への特徴的な集積が観察された。本成果により PET の分子イメージングを目的とする ^{63}Zn の利用が可能となった。

多量体ガリウム放射性薬剤としての 1,4,7-triazacyclononane-1,4,7-tris-(glutaric acid) (NOTGA)のジアステレオマーの合成と検討

「背景」ガリウム-68「^{68}Ga」は半減期 67.7 分であることから速やかな薬物動態を示す低分子化合物の標識に有用である。一方、標識プローブの設計においては、標的分子認識素子を分子内に複数分子持つ多価化合物は、標的分子認識素子を一分子しか持たない一価化合物に比べ、高い結合力を有し、これは多価効果として知られている。二

官能性キレートである NOTGA は多量体の ^{68}Ga 放射性薬剤を調整するために開発された。NOTGA は(*R*,*S*) α-bromoglutaric acid 1-tert-butyl ester 5-benzyl ester を用いて 1,4,7-triazacyclononane の窒素にアルキル化することでジアステレオマーである *RRR/SSS* と *RRS/SSR* の 2 つの鏡像異性体を生成する。そこで、これらのジアステレオマーの性質を評価するために，それぞれの NOTGA-^{t}Bu$_3$ キレート前駆体または triethylene glycol リンカー「TEG」を含む RGD ペプチド結合体を合成し、^{67}Ga による標識、および ^{67}Ga 標識体の安定性、Integrin $\alpha_v\beta_3$ の結合親和性および体内動態を比較した。

「方法と結果」NOTGA の *RRR/SSS* と *RRS/SSR* のジアステレオマーを 69%と 17%の合成収率で得た。^{67}Ga による標識反応を配位子濃度 10 μM、室温において検討した結果, *RRS/SSR* は pH 依存性を示さなかったが、*RRR/SSS* は pH 依存的に変化し pH 5 が最適であった。標識溶液 pH 5 ではいずれのジアステレオマー錯体も、10 分以内に、放射化学的収率 95%以上で得られた。いずれのジアステレオマー錯体も apo-Transferrin 溶液中で安定に存在することを確認し、標的へ同程度の結合親和性を認めた。正常マウス実験において各ジアステレオマー錯体は同様の体内動態を示し、いずれも腎臓排泄であった。また、U87MG 細胞を移植した担癌モデルマウスを用いた検討では，いずれも腫瘍に対して同程度の集積を認め、SPECT/CT 画像として鮮明な画像を与えた。

「考察」本研究成果により、NOTGA-(TEG-RGD)$_3$ 誘導体のジアステレオマーの構造学的な相違は ^{67}Ga 標識反応、または生物学的な性質に有意な影響を与えず、混合ジアステレオマー放射性薬剤の使用が可能であることを示した。しかしながら、標的分子認識素子の特異的な性質と細胞でのレセプター発現レベルや薬物動態修飾リンカーなどはジアステレオマーの構造学的な相違による分子プローブのリガンドーレセプターの相互作用または薬物動態に影響する可能性があることから、異なる標的分子認識素子に NOTGA を応用する際には誘導体の調製または化学的なおよび生物学的性質を調べることが重要であると考えられる。

「総括」陽電子放出核種である ^{63}Zn と ^{68}Ga の純粋な NOTGA ジアステレオマー分子プローブは分子イメージングにおいて新規 PET 放射性薬剤の開発に寄与すると期待できる。

Preface

In recent years, a greater understanding between disease pathogenesis and molecular alterations at cellular levels has promoted the discovery of molecules able to target these alterations.(*1, 2*) Molecular Imaging aims to use these "targeting molecules" for the visualization, characterization, and measurement of biological processes at the molecular and cellular levels.(*3*) The relevance of this discipline is not simply to study the biology underneath a disease, but to do it in a personalized approach; allowing personalized medical care based on individual specificities. In cancer patient management, one of the leading causes of dead worldwide, the diagnosis and staging of tumors, as well as, assessment of therapeutics targets, monitoring therapy and prognosis evaluation can be performed.(*1, 2*) Molecular imaging can be also applied to the process of new drug discovery or in basic science, to the discovery of new targets for diagnosis and treatment.

Radiotracer imaging by Positron Emission Tomography (PET) is one of the techniques used in molecular imaging, due to the high quantification and resolution properties of this imaging modality.(*1, 4*) PET imaging is based on the detection of the anti-parallel 511 keV gamma rays emitted from the annihilation of positrons with surrounding electrons (Figure 1 A) by detectors arranged in a ring around the subject (Figure 1 B). Only two photons detected in coincidence (10 – 20 ns) are registered, being unnecessary physical collimation to block scattered photons not perpendicular to the detector surface. Due to this "electronic" collimation PET will therefore be much more sensitive (1 – 2 orders higher) than other radiotracer based modalities, such as Single Photon Emission Computed Tomography (SPECT). The number of coincidences registered by all possible detector pairs along their respective axis provides an estimation of the number and position of the positron-emitting nuclides, hence a quantitative map of the

radiopharmaceutical concentration over time throughout the living human being.(*1*)

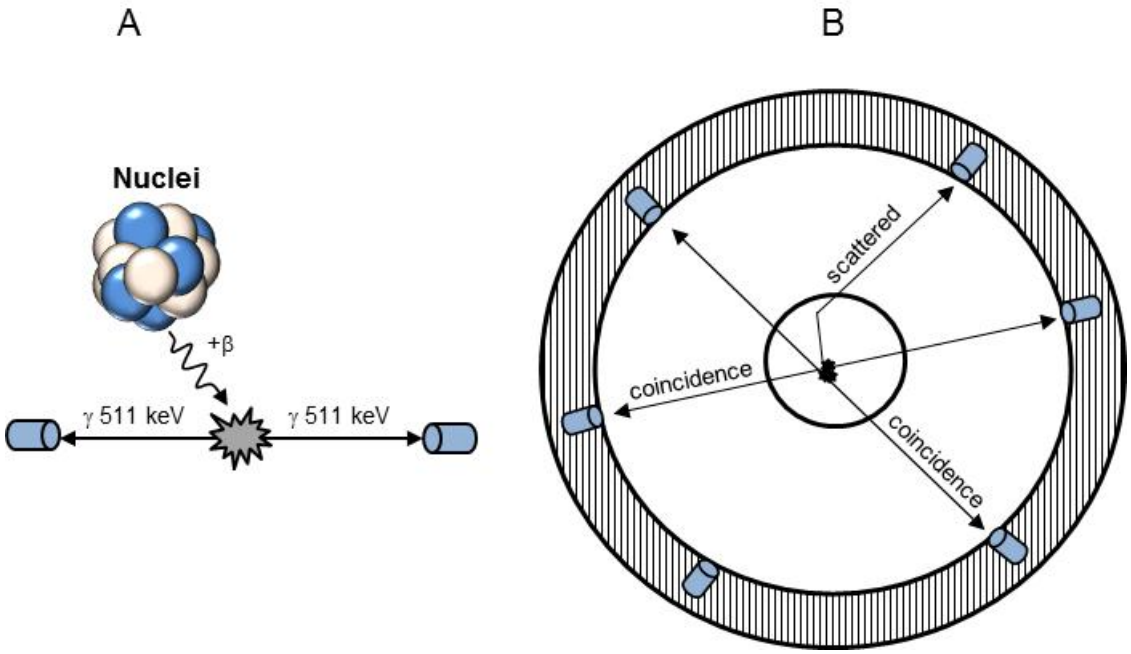

Figure 1. PET imaging basic principles. (A) The movement of the positron before annihilating with an electron, with emission of two 511 keV photons opposite to each other; and (B) a scheme depicting a PET camera with the acquisition system. Only coincident photons and not scattered are registered

PET radioisotopes are artificially produced with high specific activities in cyclotrons, as result of the nuclear reaction induced upon the irradiation of a target element with protons, deuterons, etc. The traditional PET isotopes are fluorine-18 (^{18}F), carbon-11 (^{11}C), nitrogen-13 (^{13}N) and oxygen-15 (^{15}O) (Table 1). ^{11}C, ^{13}N and ^{15}O are considered "biological" positron-emitting isotopes, since they are chemical elements normally found in biological substrates. By far ^{18}F is the most used among them, partly because its ideal decay properties, i.e. high positron abundance and low positron energy; and the success of 2-deoxy-2-[^{18}F]fluoroglucose, an FDA approved radiopharmaceutical to study drug metabolism in lung, heart, brain, and localization of tumors.

Table 1 Decay data and production routes of commonly used PET radioisotopes (*1, 5, 6*)

Nuclide	Decay Mode (%)	$T_{1/2}$	$E_{\beta+}$ keV (%)[a]	Nuclear reaction for production
^{11}C	β^+(99.8)	20.36 min	960.4 (99.80)	$^{14}N(p,\alpha)^{11}C$
^{13}N	β^+(100)	9.97 min	1199 (99.80)	$^{16}O(p,\alpha)^{13}N$
^{15}O	β^+(100)	2.04 min	1732 (99.90)	$^{15}N(p,n)^{15}O$ $^{14}N(d,n)^{15}O$
^{18}F	β^+(100)	109.8 min	633.5 (96.70)	$^{18}O(p,n)^{18}F$
^{64}Cu	β^+(17.6) EC(43.9) β^-(38.5)	12.7 h	653.0 (17.60)	$^{64}Ni(p,n)^{64}Cu$
^{68}Ga	β^+(89.1) EC(10.9)	67.7 min	1899 (87.94)	$^{68}Ge/^{68}Ga$ Generator

[a]Mean β^+ energy (total β^+ intensity)

One important aspect in the progress of molecular imaging field is the development of improved imaging probes. In PET-based radiopharmaceuticals this is translated, among others, into the production of novel radioisotopes with more desirable nuclear or chemical properties to match an intended molecular process.

In this sense, there are essential trace elements in the body, such as zinc, whose radioactive isotopes could be directly used to study biofunctions or molecular interactions where the metal plays an important role, a subject not exploited yet in molecular imaging. They can be thought as the metallic version of the "biological" radioisotopes. Zinc is a metal involved in numerous biological processes in the body (*7*) and among the useful radioactive zincs (^{62}Zn, ^{63}Zn, ^{65}Zn), ^{63}Zn possesses the most appropriate nuclear properties for PET imaging. However, the radionuclide was not available for molecular imaging purposes due to the lack of production and purification methods.

On the other hand, alternative positron-emitting radionuclides can be also obtained via generators. A representative example is the metallic radioisotope gallium-68 ($T_{1/2}$ = 67.7 min) which is available from $^{68}Ge/^{68}Ga$ generators. ^{68}Ga radiopharmacy is cyclotron-independent and allows the development of cold, freeze-dried kits that can be conveniently labeled similar to the case of $^{99}Mo/^{99m}Tc$-generators, at the workhorse in nuclear medicine. The attention gained by ^{68}Ga is evidenced by more than 50 radiopharmaceuticals enlisted in the Molecular Imaging and Contrast Agent Database (MICAD) (*8*) and the clinical success of ^{68}Ga-DOTATOC for imaging somatostatine receptors in neuroendocrine tumors.(*9, 10*)

One major advantage of metallic radioisotopes like ^{68}Ga is their simpler radiolabeling, governed by their coordination chemistry. It allows the development of bifunctional chelators (BFC), which are in essence chelators equipped with functional groups for both, conjugation of a biomolecule of interest and coordination of the metal cation. Therefore, a metal containing molecular probe consists of a radionuclide wrapped by the BFC, the targeting molecule and additionally a pharmacokinetic modifier (PkM) linker is sometimes included (Figure 2).(*11*)

Novel BFCs for gallium that improve aspects of molecular design such as, conjugation of biomolecules, radiolabeling or implementing innovative targeting strategies to increase probe avidity, have been developed.(*12-15*) One example is 1,4,7-triazacyclononane-1,4,7-tris-(glutaric acid) (NOTGA). This BFC possesses a 1,4,7-triazacyclononane (TACN) core structure with three glutaric acid pendant arms; and it was designed to allow multiple conjugation of targeting molecules as a way to exert the multivalent effect,(*16, 17*) a targeting strategy used in receptor-based imaging for maximizing binding capabilities.(*11, 18-21*) One peculiarity in NOTGA is the presence of three chiral centers located at the alpha position of each glutaric acid moieties, leading to the formation of two diastereomeric pairs of enantiomers. However, their

isolation and the influence their structural differences, which might affect the stability, radiochemistry, target affinity, pharmacokinetics and in vivo targeting properties, have not been study yet.

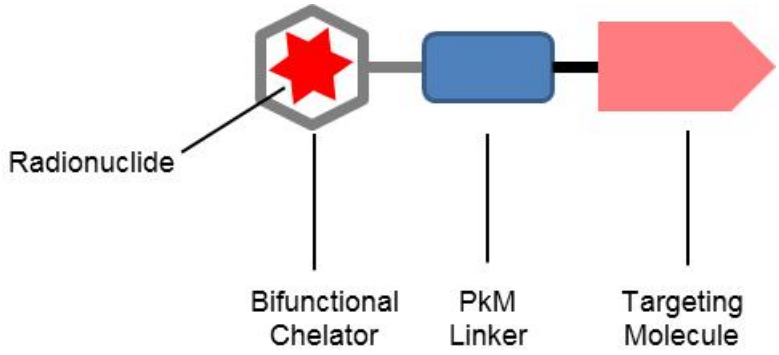

Figure 2. Molecular probe design of a metal-based radiopharmaceutical. PkM (Pharmacokinetic Modifier)

With all above in mind, it is the intention of the present thesis to tackle two important aspects of the development of PET-based radiopharmaceuticals: first, the radioisotope production, materialized in the development of a method for the production and purification of the metallic positron emitting radionuclide zinc-63; and second, the molecular probe design, exemplified in the synthesis and evaluation of diastereomers of NOTGA for the preparation of multimeric radiopharmaceuticals of gallium.

The first topic is addressed in Chapter 1 entitled "Production and purification of the positron emitter zinc-63". The *Introduction* section makes a summary of the role of zinc in the human body and the applications that radioactive zinc has found so far. It also presents the advantages of ^{63}Zn over the analogues ^{62}Zn and ^{65}Zn and the irradiation of copper targets with protons as the most convenient ^{63}Zn production route. *Materials and methods* section gives details of the

irradiation protocol, the purification system based on cation exchange chromatography, including a detailed scheme, and the analytical methods used to assess the purity of the ^{63}Zn final solutions. Issues such as, proton energy selection, copper target thickness and its impact on the following purification step are addressed in *^{63}Zn production* of the *Results and Discussion*. In the same section, the efficacy of the purification method to save elution time to avoid decay of the ^{63}Zn product, and to provide high purity final product is analyzed in *Radiochemical processing of ^{63}Zn*. Further, the applicability of the ^{63}Zn was estimated in a PET imaging study. The chapter finishes with the partial conclusions.

Chapter 2 presents the "Synthesis and evaluation of diastereoisomers of 1,4,7-triazacyclononane-1,4,7-tris-(glutaric acid) (NOTGA) for multimeric radiopharmaceuticals of gallium". *Introduction* section makes a brief summary of the nuclear properties and coordination chemistry of gallium radioisotopes important to imaging, aspects related to TACN-based BFC designed for multi-attachment of biomolecules and the formation of stereoisomers are also revised. The possibility of preparation of diastereomerically pure NOTGA radiopharmaceuticals is postulated and a RGD peptide molecular probe is formulated to address the problem. The synthetic procedures and other in vitro and in vivo experiments protocols are presented in *Materials and Methods*. A whole section devoted to *Results* includes, among others, the isolation of isomers of NOTGA, ^{67}Ga radiolabeling, stability, in vitro affinity for integrin $\alpha_v\beta_3$, and animal experiments. The results are analyzed and discussed in relation to the existing international knowledge in the *Discussion* section. *Conclusions* to this chapter are also given. *General Conclusions* will integrate the achievements of the thesis from a global point of view and references will be gathered in the *Bibliography* section.

Index

Chapter 1.

Production and Purification of the Positron Emitter Zinc-63

1.1. Introduction

Zinc is one of the essential trace minerals in the body, and is required for the metabolic activity of more than 300 enzymes. It is also involved in protein, nucleic acid, carbohydrate, and lipid metabolism, as well as in the control of gene transcription and other fundamental biological processes.(*7*) Zinc deficiency and perturbations of zinc metabolism are now recognized as factors in the pathogenesis of several chronic diseases.(*22*)

Although the potential use of ^{63}Zn-EDTA was reported in 1974,(*23*) the application of radioactive zinc for imaging purposes has been limited to ^{62}Zn and ^{65}Zn. They have been used for preparing pancreas-seeking radiopharmaceuticals,(*24-27*) labeling an anti-cancer agent, (*28, 29*) and brain tumor imaging.(*30-34*)

Table 1.1 Decay data of zinc radioisotopes (*6*)

Parent Nucleus	Decay mode	$T_{1/2}$	$E_{\beta+}$ keV (%)[a]	Daughter Nucleus
$^{62}_{30}Zn$	EC, β^+	9.26 h	259 (8.40)	$^{62}_{29}Cu$
$^{63}_{30}Zn$	EC, β^+	38.47 min	992 (92.7)	$^{63}_{29}Cu$
$^{65}_{30}Zn$	EC, β^+	243.93 d	143 (1.42)	$^{65}_{29}Cu$

[a]Mean β^+ energy (total β^+ intensity)

However, these zinc radioisotopes present some drawbacks as radionuclides for PET imaging. ^{62}Zn is a positron emitter with a half-life of 9.26 h, which decays to another positron emitter, ^{62}Cu, with 9.7 min of half-life. This constitutes a source of non-isotopic radionuclidic impurity. The long half-life of ^{65}Zn, on the other hand, would result in unacceptable radiation exposure to patients, which significantly hinders its clinical application (Table 1.1). Furthermore, the positron emission intensity of both radioisotopes is rather low. Conversely, ^{63}Zn decays to the stable ^{63}Cu with a half-life of 38.47 min and has high positron abundance (Table 1.1). Such nuclear properties render ^{63}Zn an attractive radionuclide for molecular imaging to better understand the role played by the metal in the body through PET imaging. However, the application of ^{63}Zn has been unexplored, because of the lack of methods for the production and purification of non-carrier added (n.c.a) ^{63}Zn.

^{63}Zn can be produced by irradiating natural copper with protons through the ^{nat}Cu(p,n)^{63}Zn nuclear reaction that exhibits high cross section values at low proton energies.(*35*) Although the ^{60}Ni(α,n)^{63}Zn nuclear reaction exhibits comparable cross sections,(*36*) the coproduction of ^{62}Zn is inevitable, making its application difficult. ^{63}Zn can also be produced from the irradiation of natural zinc with neutrons thorough the ^{64}Zn(n,2n)^{63}Zn;(*23*) however, the reaction produces ^{63}Zn in a carrier-added form. In this study, the production of ^{63}Zn through the irradiation of natural copper targets with proton beams, its subsequent purification by ion exchange chromatography, as well as a pilot PET imaging study is presented.

1.2. Materials and methods

1.2.1. General

Copper foils (100 μm in thickness, 99.99 % purity) were purchased from Fuchikawa Rare Metal Co. (Tokyo, Japan). Analytical grade ion exchange resin (AG 50W-X8, H^+ form, 100-200 mesh) was obtained from Bio-Rad Laboratories, Inc (Tokyo, Japan). Reagents used in standard productions were analytical grade from Wako Pure Chemical Industries, Ltd (Osaka, Japan) and used without further purification. Water was purified using a Milli-Q purification system. To reduce the amount of metal impurity ultra-pure grade conc. Nitric acid, conc. HCl and water were purchased from Wako Chemicals and; acetone was purchased from Kanto Chemical Co., Inc (Tokyo). Proton energy calculations were performed using the software SRIM.exe 2008-3 (*37*) or stopping power formulas.(*38*) The primary beam energy (14 MeV nominal) was checked using the ratio $\sigma_{65Zn}/\sigma_{63Zn}$ determined experimentally from the $^{nat}Cu(p,x)^{63,65}Zn$ nuclear reactions in a copper foil of 20 μm thickness (*39*) (13.93 ± 0.12 MeV experimental). Cross-section data was taken from IAEA TECDOC 1211.(*35*)

1.2.2. Production of ^{63}Zn via $^{nat}Cu(p,n)^{63}Zn$ reaction

The irradiations were carried out using protons of 14 MeV from the AVF-930 cyclotron of the National Institute of Radiological Sciences of Japan, at beam intensities of 0.5 – 8 μA for 0.5 – 1.5 h. A stack of 1.9 cm in diameter was arranged using an aluminum foil of 70 μm thickness to degrade the energy from 14 MeV to 13.5 MeV and the copper target of 100 μm thickness (13.5 → 11.4 MeV). After irradiation, the target holder was removed from the irradiation port and transferred to a shielded hot cell where all the operations were performed

remotely.(*40*)

1.2.3.Purification of ^{63}Zn from the Cu target

The purification of ^{63}Zn was carried out using the apparatus shown in Figure 1.1. The irradiated Cu foil was dropped inside the dissolution vessel using mechanical arms. The HNO_3 (1.5 mL) was added to the vessel from the A Line. After complete dissolution of the foil, water (15 mL) was added from the B Line and the solution was bubbled with air. The solution was loaded onto a cation exchange resin column (AG 50W-X8, H^+ form, 1 cm I. D. × 40 cm, preconditioned with water) using a peristaltic pump. The column was then washed with 10 mL of water (from the D line). Lastly, ^{63}Zn was eluted with a mixture of 0.05 N HCl – 85% acetone solution (prepared by mixing 0.33 M HCl and acetone at 1:5.7 v/v ratio) from the C line at a flow rate of approximately 3.5 mL/min. The eluents were monitored using the radiation sensor (RS). Radioactive fraction was collected and concentrated to dryness to remove HCl using a rotary evaporator. After the radioactive solution was evaporated to dryness, the residue was re-dissolved in 5 – 10 mL of H_2O or saline.

1.1.1.Analysis of final product solutions

The radioactivity was determined both destructively and non-destructively by standard gamma-ray spectrometry using a HpGe detector Gx1020 (4098 channels, 0.9 keV/channel, 34 – 3643 keV) manufactured by Canberra Industries, Inc, CT, USA coupled to the acquisition system RZMCA 1.1.0.3 (Laboratory Equipment Corporation, Ibaraki, Japan) as well as a dose calibrator (ICG-3, ALOKA CO., LTD, Tokyo), which was cross-calibrated with the HpGe detector. The energy and efficiency calibration of the HpGe system was done using a ^{152}Eu

certified calibration source obtained from Japan Radioisotope Association (Tokyo); and ^{137}Cs and ^{60}Co standard sources from QSA Global Inc. (Burlington, USA) (error < 3 %). Gamma ray energies and intensities for calibration were taken from the Nudat database.(*6*) The detector-source distance was kept high enough to avoid summation of the pulses originating from cascade processes and dead times of less than 5 %.

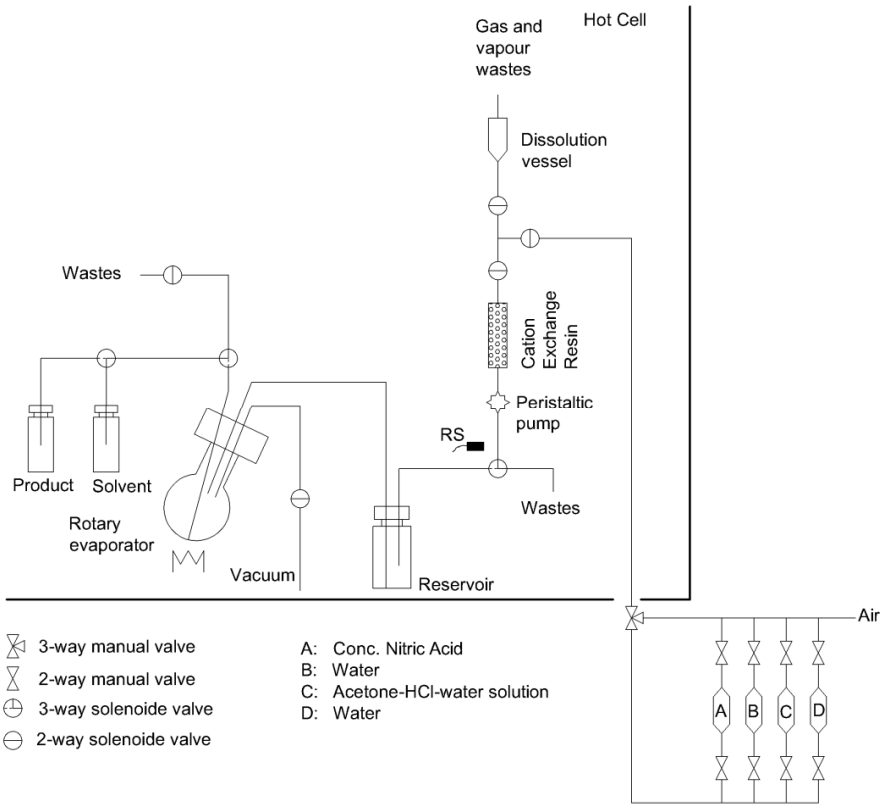

Figure 1.1. Apparatus used for the production of ^{63}Zn from the copper target. (RS: Radiation sensor)

The final ^{63}Zn solutions were analyzed also by high performance ion exchange chromatography coupled to a UV–Vis detector (2475, Waters Corporation, Milford, MA, USA) and a NaI(Tl) radioactivity detector (Ohyo Koken Kogyo Co; LTD, Tokyo). The metal analysis was performed by ion chromatography with post column method. Samples were analyzed on a

column (IonPac CS5A, 4 mm I.D. × 250 mm; Dionex K.K., Osaka) equipped with a guard column (IonPac CG5A, 4 mm I.D. × 50 mm, Dionex K.K., Osaka) with mobile phase of diluted MetPac PDCA (Dionex K.K, Osaka) (MetPac PDCA : H_2O = 1 : 5) at a flow rate of 1.2 mL/min. MetPac PDCA represents 7 mM of pyridine-2,6-dicarboxylic acid, 66 mM of potassium hydroxide, 5.6 mM of potassium sulfate and 74 mm of formic acid. The eluents from the column were mixed with a post column reagent, 4-(2-pyridylazo) resorcinol (PAR) in MetPac eluent (0.06 g/L), at a flow rate of 0.6 mL/min. MetPac represents 1 M of 2-dimethylaminoethanol, 0.5 M of ammonium hydroxide and 0.3 M of sodium bicarbonate solution The mixture was monitored at 530 nm. The lower limits of detection of the elements were 0.020 μg/g (Fe), 0.125 μg/g (Ni), 0.020 μg/g (Co), 0.019 μg/g (Cu) and 0.018 μg/g (Zn).

1.1.2.Small-animal PET scanning

Male Wistar rats (8 weeks old) were obtained from Japan SLC (Shizuoka, Japan). The animal experimental procedures were approved by the Animal Ethics Committee of the National Institute of Radiological Sciences. A chest/abdominal PET scan was performed using small-animal PET scanner, Inveon^{TM} (Siemens Medical Solutions USA, Knoxville, TN), which provides 159 transaxial slices 0.796 mm (center-to-center) apart, a 10 cm transaxial field of view (FOV), and a 12.7 cm axial FOV.(*41*) Prior to the scan, the rat was anesthetized with 5% (v/v) isoflurane, and maintained thereafter by 1–2% (v/v) isoflurane. After transmission scans for attenuation using a Cobalt-57 point source, emission scan was acquired for 60 min after intravenous injection of [^{63}Zn]$ZnCl_2$ (16 MBq, 0.3 mL). All list-mode acquisition data were sorted into 3-dimensional sinograms, which were then Fourier rebinned into 2-dimensional sinograms (frames × min; 4 × 1, 8 × 2, 8 × 5). Dynamic images were reconstructed with filtered back-projection using Hunning's filter, and a Nyquist cutoff of 0.5 cycle/pixel.

1.3. Results and Discussion

1.1.3. ^{63}Zn production

^{63}Zn can be formed from natural copper (^{63}Cu, 69.2%; ^{65}Cu, 30.8%) via two nuclear reactions: ^{63}Cu(p,n)^{63}Zn with a threshold energy of E_{th} = 4.2 MeV, and ^{65}Cu(p,3n)^{63}Zn, with E_{th} = 22.3 MeV. The highest cross section values (probability of the reaction to occur) of the $^{63/65}$Cu(p,n)^{63}Zn reaction are attained at a proton energy range between 16 to 6.5 MeV with a maximum at proton energy of 12.55 MeV. Unfortunately, within this useful energy region, both ^{62}Zn and ^{65}Zn are also produced (Figure 1.2). Hence, careful selection of the initial proton energy was needed in order to minimize impurities. The generation of undesired ^{62}Zn was completely avoided at proton energy levels below 13.47 MeV, the threshold energy of the ^{63}Cu(p,2n)^{62}Zn reaction.

The yield of ^{63}Zn increases as incident energy range increases using thick targets. However, the use of thick copper targets requires larger columns in the purification process, which result in longer purification times to remove the target. Therefore, a favorable balance between the target thickness and purification time (i.e. yields at the end of bombardment (EOB) and at the end of processing) is necessary. The consideration led us to select a target thickness of 100 μm for an energy range from 13.5 to 11.4 MeV (Figure 1.2), thereby covering the highest cross-section values for a theoretical yield of 1.87 GBq/μA·h. This is a production parameter that is calculated using the relationship: $Y = \lambda \times N_{atoms} \times N_{proton} \times \sigma(E)$ integrated over the energy range and expressed in $\left[\frac{Bq}{\mu A \cdot h}\right]$. The product of the number of target atoms (N_{atoms}), the number of incident protons (N_{proton}) and the cross-section (σ) gives the number of product atoms formed,

that multiplied by the disintegration constant ($\lambda = \frac{\ln 2}{T_{1/2}}$) gives the activity of the sample (in *Bq*). The number of protons N_{proton} is conveniently expressed in 1/μA·h for practical reasons. It can be observed that long-lived radionuclides will have low yields. Nevertheless, experimentally the production yield is calculated from the measured activity following the relationship: $Y = \frac{Activity}{I} \times \frac{\lambda}{\left(1 - e^{-\lambda T}\right)}$. Where *I* (in μA) is the beam intensity and *T* (in *h*) is the irradiation time.

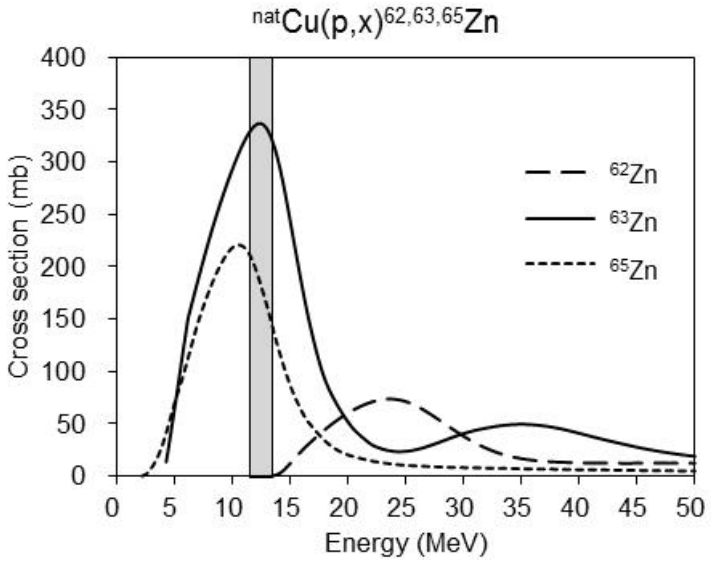

Figure 1.2. Reaction cross-section of zinc radioisotopes in proton irradiated copper (*35*)

The experimental thick target yields determined from trial irradiations are presented in Table 1.2. The average was 1.41 ± 0.19 GBq/μA·h, which is 75.4 % of the predicted value and some deviation was observed in one of the experiments. Since the energy was found to be in agreement with the nominal value, factors such as variations in the current delivered by the cyclotron, beam alignment, uncertainty in the activity determination, etc., might affect the results. Irradiated targets were allowed to decay and the radioactivity was measured. Although

the formation of ^{62}Zn was completely avoided, the gamma spectrometry analysis of the copper targets revealed the presence of ^{65}Zn and ^{64}Cu impurities. The resulting yields were 91 ± 9.3 kBq/μA·h for ^{65}Zn and 164 kBq/μA·h for ^{64}Cu. ^{65}Zn is formed only from ^{65}Cu via the ^{65}Cu(p,n)^{65}Cu reaction with a threshold energy of E_{th} = 2.2 MeV. Meanwhile, ^{64}Cu is formed from the nuclear reaction ^{65}Cu(p,n+p)^{64}Cu with E_{th} = 10.06 MeV. Thus, the use of ^{63}Cu-enriched targets would allow producing ^{63}Zn not only in high yields but also in high purities since ^{65}Zn and ^{64}Cu would be minimized.

Table 1.2. Experimental thick target yields of ^{63}Zn[a,b]

Run #	μA	min	^{63}Zn Yield (GBq/μA·h)	% of theoretical yield[c]
1	0.50	30	1.68	89.9
2	0.50	30	1.34	71.4
3	1.0	30	1.37	73.0
4	0.50	30	1.26	67.3

[a] Ep= 13.5 → 11.4 MeV
[b] Non-destructive measurements
[c] Calculated yield: 1.87 GBq/μA·h

1.1.4. Radiochemical processing of ^{63}Zn

Due to the relatively short half-life of ^{63}Zn ($T_{1/2}$ = 38.47 min), a short and efficient separation process was required to minimize the loss by the decay of the product and by purification process. Typical procedure to separate zinc from copper through an anion exchange column chromatography is time-consuming (ca. 2 h), (*40*) as the radioactive zinc elutes after the elution of the copper target. To reduce purification time, a different elution system that elutes first the product while keeping the copper target in the column was appropriate.

Strelow et al. reported distribution coefficients with cation exchange resin for several metal ions in HCl – acetone mixture. High distribution coefficient ratio for Cu^{2+}/Zn^{2+} pair of 76 is achieved using a 0.1 N HCl – 80% acetone.(*42*) Under the conditions, ^{63}Zn was obtained in the first elution fractions while keeping the bulk copper target in the column. It was also documented that at low acid concentrations, the distribution coefficients increase as the acetone concentration increases, until the hydration field around the cation is weak enough to allow the replacement of the water dipoles in the coordination shell by chloride anions.(*42*) Considering that low acid concentration and high acetone concentration were favorable conditions for accelerating the evaporation step and avoiding polymerization of acetone by HCl, the elution conditions were also performed using a combination 0.05 N HCl – 85% acetone. Since the two elution conditions resulted in similar copper contents in the ^{63}Zn fractions, the elution system utilizing 0.05 N HCl-85% acetone was selected to purify ^{63}Zn from the copper target by cation exchange chromatography.

In practical productions, the target foil readily dissolved in nitric acid was loaded onto the column without further rinsing the dissolution vessel. Radioactivity was detected between 20 and 30 minutes after loading the metal solution and the radioactive fraction corresponding to the ^{63}Zn radionuclides was collected (70 – 80 mL), as shown in figure 1.3. Approximately 93.3 % of the loaded activity was recovered in the solution. However, losses during processing (9 % and 35 % of the radioactivity remained in the dissolution and evaporation vessel respectively) impacted the yield of HCl free ^{63}Zn solutions. The chemical processing lasted an hour and the $^{63}ZnCl_2$ final product was ready to use at 1.6 h after EOB.

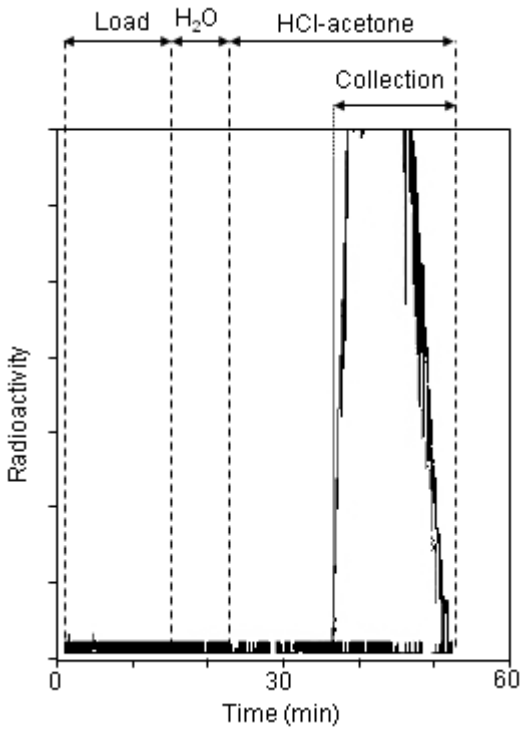

Figure 1.3. Radioactivity content in the effluents (expressed in arbitrary units)

Table 1.3. Irradiation parameters, yield and purity analysis of practical production [a]

Run #	μA	min	^{63}Zn Yield MBq/μA·h[a]	% predicted[a]	Purity (%)	SPA GBq/μmol[a]	Metal Impurity (μg)[b]
1.	8.0	60	166	44.8	99.92	29.4	Zn^{2+} 1.8, Cu^{2+} 0.2, Fe^{2+} 0.8, Co^{2+} 0.15
2.	8.0	60	156	42.1	99.91	5.65	Zn^{2+} 7.1, Cu^{2+} 0.2, Fe^{2+} 1.7
3.	6.0	90	145	39.3	99.91	4.66	Zn^{2+} 9.1, Cu^{2+} 0.1, Fe^{2+} 1.4
4.	5.0	30	221	59.7	99.94	2.39	Zn^{2+} 11.8, Fe^{2+} 10.2
5.	5.0	30	159	43.0	99.54	1.79	Zn^{2+} 11.2, Cu^{2+} 1.2, Fe^{2+} 1.9

[a] Specific activity (SPA). Referred to the End of Processing
[b] Metal content per 5 mL of water/saline

The results of the productions are presented in Table 1.3. The average yield of the purified ^{63}Zn at the end of processing was 169 ± 30 MBq/μA·h, i.e. 45.8 % of the predicted value. The radionuclidic purity was higher than 99%, with ^{65}Zn being the only impurity. ^{64}Cu was not detected after the purification (Figure 1.4).

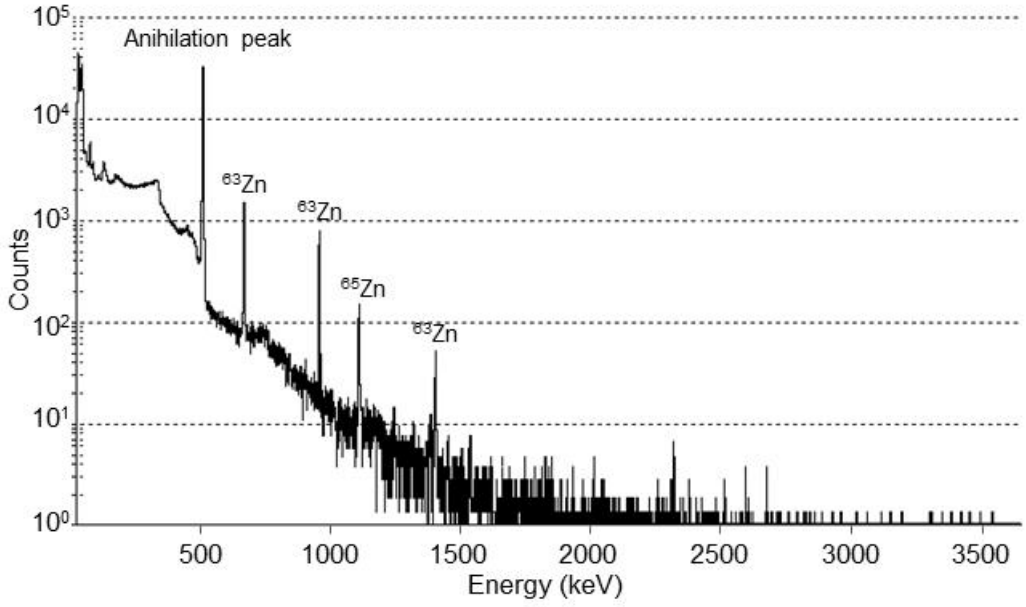

Figure 1.4. Gamma spectrum of the ^{63}Zn final product. HpGe detector (30 cm of source – detector distance, LT 1128 sec). Gamma lines: ^{63}Zn: 669.6 keV (8.2%), 962.1 keV (6.5%), 1412.1 keV (0.75%); ^{65}Zn: 1115.5 keV (50.6%)

The HPLC-IC analyses detected Fe^{3+}, Cu^{2+}, Co^{2+} and Zn^{2+} (Table 1.3). The copper concentration could be decreased to 0.04 μg/g and the only radioactive ion detected was Zn^{2+} (Figure 1.5). However, the amounts of non-radioactive zinc were relatively high at the initial experiments (1.42 – 1.82 μg/g). The carrier zinc could come from several sources, including the copper target, the reagents used and contamination in the purification apparatus. When analytical grade reagents were changed to ultra-pure grade reagents, including water, and thoroughly cleaning of the production system was performed, the zinc amount decreased by a

factor of 5 for a specific activity of 29.4 GBq/μmol at 1.5 h EOB. Low specific activity may constitute a limiting factor for biological studies. Since the copper target impurities are a source of contaminant zinc, a reduction of the target size and use of highly pure ^{63}Cu enriched targets would increase the specific activity.

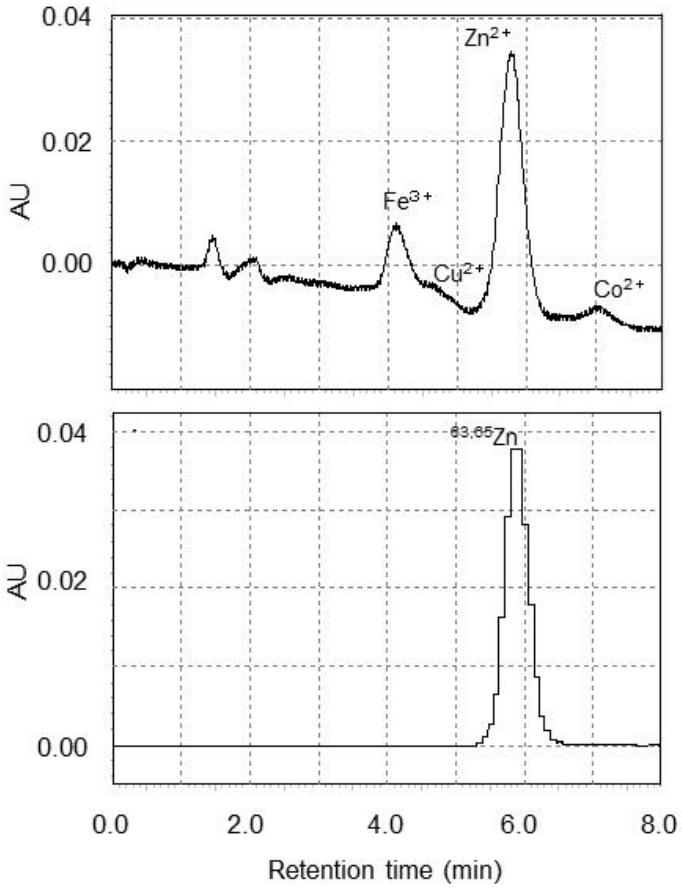

Figure. 1.5. Ion chromatograms of ^{63}Zn solutions. (Fe^{3+}: 4.25 min, Cu^{2+}: 4.84 min, Zn^{2+}: 6.05 min, Co^{2+}: 6.84 min). (AU: arbitrary units)

1.1.5. Animal PET study

The applicability of the presently produced ^{63}Zn for molecular imaging was estimated in a PET imaging study performed 1 h after injection of [^{63}Zn]$ZnCl_2$ to a male Wistar rat (Figure 1.6). Radioactivity was observed in the liver and kidneys, in good agreement with tissue

distribution studies previously reported using the radioisotope ^{65}Zn.(*26, 43-45*) Furthermore, accumulation was also observed in pancreas, attributable to the utilization of the metal for exocrine functioning, in carboxypeptidase enzymes;(*24, 25*) and endocrine functioning, in the synthesis of insulin (*46-48*) thanks to the presence of zinc transporter in the tissue.(*49, 50*) These studies indicated that the presently produced ^{63}Zn met the laboratory necessity for molecular imaging with PET. Recent efforts are being made to estimate beta-cell mass by non-invasive in vivo imaging for better understanding the diabetes pathogenesis and monitoring therapeutic recovery of the cell.(*51*) The findings in this study along with previous ones using $^{62/65}$Zn (*24-27, 43, 52, 53*) imply that ^{63}Zn would be useful for estimating pancreatic functions by PET imaging. Additionally, zinc and its transporters are involved in a variety of biological processes in the body and alterations are related to chronic pathologies such as, Alzheimer's disease (*7, 22*) that could be investigated using ^{63}Zn.

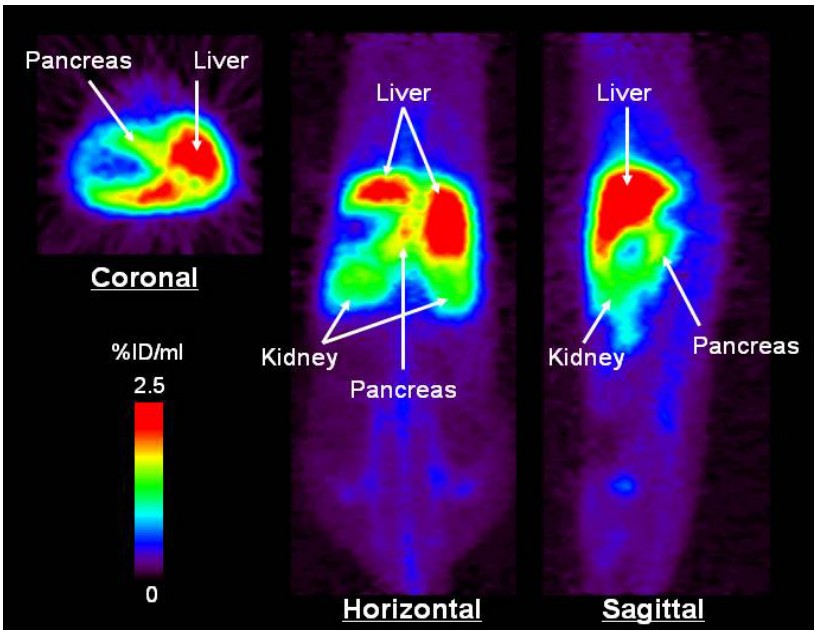

Figure 1.6. Representative chest/abdominal PET images of [^{63}Zn]Zn (16 MBq) in the isoflurane-anesthetized rat. PET images were generated by summation of the whole scan (0–60 min). %ID/ml (Percentage of injected dose per ml)

1.4. Conclusions

The production and purification of the PET radionuclide ^{63}Zn was established. The procedure was rapid and straightforward, and the product was obtained in high chemical and radiochemical purities. The typical accumulation of zinc in liver and kidneys, as well as in the pancreas, was observed in the PET image study. Therefore, the presently produced ^{63}Zn has become available for molecular imaging with PET.

Chapter 2.

Synthesis and Evaluation of Diastereoisomers of 1,4,7-triazacyclononane-1,4,7-tris-(glutaric acid) (NOTGA) for Multimeric Radiopharmaceuticals of Gallium

2.1. Introduction

Gallium radioisotopes are of great interest for molecular imaging. Gallium-68 (^{68}Ga) is a PET radioisotope available from long-lived ^{68}Ge/^{68}Ga generator systems allowing potentially cost-effective production of ^{68}Ga radiotracers far away from a cyclotron facility. Its physical half-life of 67.7 min is attractive for labeling low molecular weight probes with rapid pharmacokinetics.(*54*)

For preparing ^{68}Ga-based radiotracers, a macrocyclic chelator 1,4,7-triazacyclononane-*N,N',N''*- triacetic acid (NOTA, Figure 2.1 A) is preferably used due to the formation of a hexadentate gallium complex of high thermodynamic (Log K = 30.98) (*55*) and kinetic stabilities arising from the good fit of the relatively small gallium cation in the cyclic cavity.(*54*) Moreover, this chelator has been efficiently radiolabeled with ^{68}Ga, even at room temperature.(*13, 56, 57*)

Since the conjugation of targeting molecules to the carboxylic acids of NOTA compromises its coordination ability with Ga, several NOTA-based bifunctional chelating agents (BCA) with dissimilar functional groups in a pendant arm or on an ethylene bridge have been developed.(*12-15*) Triazacyclononane (TACN) has been selected as the core of the scaffold containing phosphinic acid (triazacyclononane phosphinic acids; TRAP) (*58, 59*) or glutaric acid (nonane triglutaric acid; NOTGA) (*16, 17*) for multi-attachment of biomolecules to the three pendant arms as a way to apply to the multivalent concept (Figure 2.1 B and C).

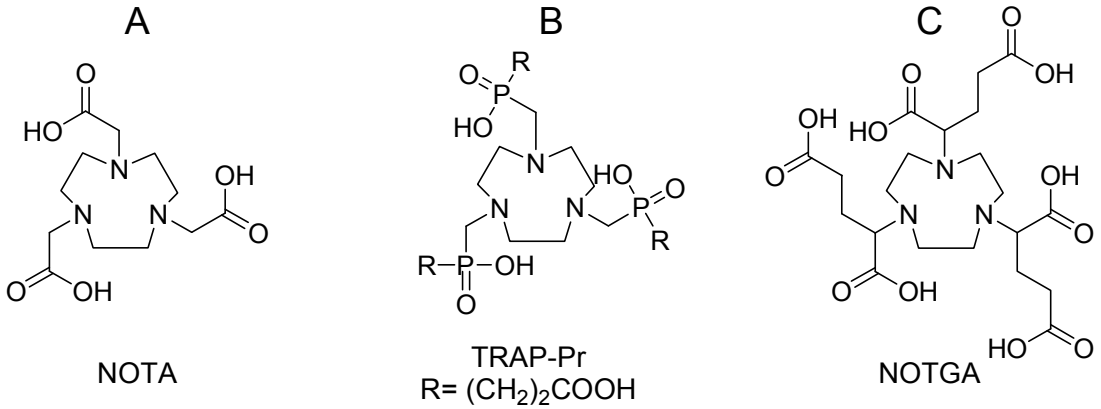

Figure 2.1. Structures of (A) NOTA and the NOTA-based BCAs, (B) TRAP and (C) NOTGA. TRAP contains phosphinic acids whereas NOTGA glutaric acids

Recently, Singh et al.(*17*) exemplarily demonstrated that the binding affinity and tumor accumulation of a trivalent cyclic RGD peptide conjugated-NOTGA (^{68}Ga-**3**) increased with respect to its bivalent and monovalent counterparts. Similarly, Notni et al. reported that the targeting ability of the trivalent ^{68}Ga-TRAP(RGD)$_3$ was superior to that of the monovalent ^{18}F-Galacto-RGD.(*59*) However, one aspect to consider when preparing NOTGA- and TRAP-based radiopharmaceuticals is the presence of chiral centers in their pendant arms leading to *RRR*, *SSS*, *RRS*, *SSR* stereoisomers. In NOTGA, these stereoisomers are formed as a result of the alkylation of TACN with racemic (*R*/*S*) α-bromoglutaric acid diester (Figure 2.2), which was also observed in the alkylation of tetraazacyclododecane,(*60, 61*) where the *RRRR* isomer of gadolinium complex exhibited faster water exchange rate than the other isomers.(*61*)

In TRAP ligands, the phosphorous atoms become chiral upon coordination with the metal ion and four *RRR*, *SSS*, *SSR*, *RRS* isomers are formed depending on the substituent.(*58, 62*) A mixture of diastereomers, with differences in spatial orientation of the chelating unit or targeting molecules and physicochemical properties, might influence the biodistribution of the molecular probe.(*63, 64*) In cases where radiopharmaceuticals can form distinct isomeric species, it is

important to evaluate the individual product separately to ensure that they both possess good biological efficacy,(*63*) as well as stability and radiochemistry.

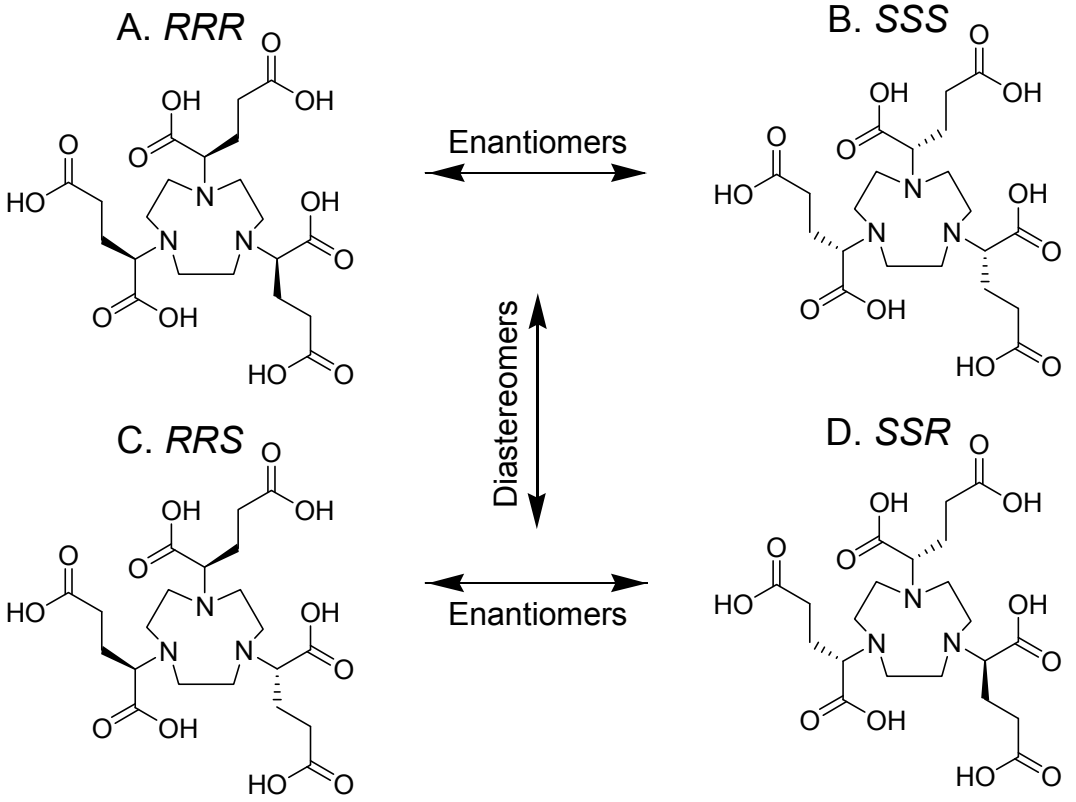

Figure 2.2. Structures of the isomeric forms of NOTGA. The *RRR* and *SSS*, as well as *RRS* and *SSR* constitute enantiomers; while the pairs *RRR*/*SSS* and *RRS*/*SSR* are diastereomers

In TRAP-based radiolabeled probes, separation of a potential diastereomer can only be conducted after radiolabeling reaction. On the other hand, the isolation of diastereomers in NOTGA is feasible after alkylation of TACN, and diastereomerically pure conjugates can be obtained. In NOTGA-based radiolabeled probes, therefore, a diastereomerically pure ^{68}Ga-labeled compound can be obtained without post-labeling purification by selecting a diastereomer of preferable chemical and biological performance. In the present study, pure diastereomers of NOTGA using RGDfK as the targeting molecule, were synthesized, and compared their performance in terms of radiochemical yields using the more convenient ^{67}Ga

($T_{1/2}$ = 3.3 d), kinetic stability, affinity for integrin $\alpha_v\beta_3$, and biological behavior of each complex in normal and nude mice bearing U87MG tumor xenografts.

2.2. Materials and Methods

2.2.1. General

All commercially obtained chemicals were of analytical grade and used without further purification. 9-Fluorophenylmethoxycarbonyl (Fmoc)-protected amino acids and H-Gly-2-Cl-Trt Resin were purchased from Watanabe Chemical Industries, Ltd. (Hiroshima, Japan). $^{67}GaCl_3$ was supplied by FUJIFILM RI Pharma Co., Ltd. (Tokyo, Japan). 1,4,7-Triazacyclononane (TACN) was purchased from Sigma Aldrich Chem. Co. (Milw, WI, USA). Apo-Transferrin (apo-Tf) Iron free was purchased from Nacalai Tesque Inc. (Kyoto, Japan). Reversed phase (RP) HPLC was performed with a Cosmosil 5C_{18}-AR-300 column (4.6 mm I.D. × 150 mm, Nacalai Tesque Inc.) at 1 mL/min with a gradient mobile phase starting from 90% A (0.1% aqueous trifluoroacetic acid (TFA) and 10% B (acetonitrile with 0.1% TFA) to 70% A and 30% B at 30 min. The eluent was monitored online with a UV-Vis single beam spectroscopy detector (L-7405, Hitachi Co. Ltd., Tokyo) coupled to a NaI(Tl) radioactivity detector (Gibi star, Raytest, Strubenhardt, Germany). TLC analyses was performed with silica plates (Silica gel 60 F_{254}, Merck Ltd., Tokyo) developed with MeOH/0.1 M $AcONH_4$ (1:1). Radioactivity was measured using a MiniGita Star Gamma TLC Scanner (Raytest) and an auto well γ counter (ARC-380M, Aloka, Tokyo). Mass spectrometry was carried out using an Agilent 6130 Series Quadrupole LC/MS electrospray system (Agilent Technologies, Tokyo) or MALDI TOF MS Kratos Axima CFR Plus (Shimadzu Corporation, Kyoto). ^{1}H, ^{13}C-NMR spectra were recorded on a *JEOL* JNM-*ECP*-400 (400 MHz) spectrometer (JEOL Ltd., Tokyo).

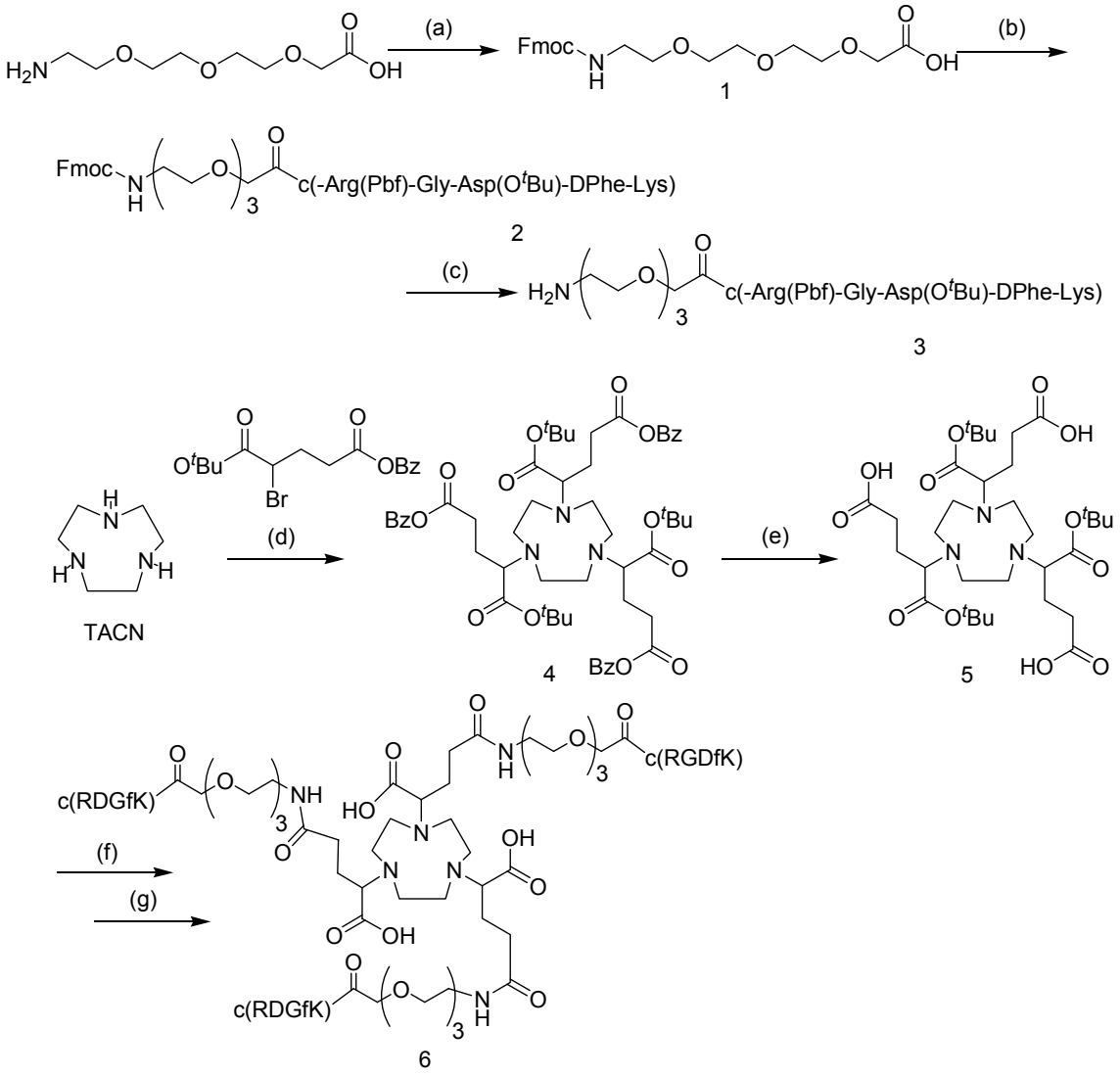

Scheme 2.1. Synthesis of NOTGA-(TEG-RGD)$_3$: (a) Fmoc-O-Su, K_2CO_3, H_2O; (b) c(-Arg(Pbf)-Gly-Asp(O^{t}Bu)-D-Phe-Lys-), EDC, HOBt, DMF; (c) 10% piperidine/DMF; (d) 1,4,7-triazacyclononane, K_2CO_3, MeCN; (e) 10% Pd/C, MeOH, H_2O; (f) H_2N-TEG-c(R(Pbf)GD(O^{t}Bu)fK), EDC, DIMAP, CH_2Cl_2; (g) TFA/ H_2O /Et_3Si

2.2.2.Synthetic procedures

(2-{2-[2-(9H-Fluoren-9-ylmethoxycarbonylamino)-ethoxy]-ethoxy}-ethoxy)-acetic acid (1) (Fmoc-TEG). 11-Amino-3,6,9-trioxaundecanoic acid (0.79 g, 3.79 mmol) and K_2CO_3 (1.04 g, 7.50 mmol) were dissolved in 5.8 mL of water and stirred at room temperature for 15 minutes

after which N-(9-fluorenylmethoxycarbonyl) succinimide (1.28 g, 3.79 mmol) was added and the mixture was stirred for 24 h, while the progress of the reaction was monitored by TLC ($CHCl_3$/MeOH/AcOH, 5/1/0.06). The salt was filtrated and the filtrate was washed with 3 × 3 mL of Et_2O, acidified to pH 1 using 3 N HCl and the desired compound extracted with 5 × 5 mL of CH_2Cl_2. After removing the solvent in vacuo, the residue was purified with open column chromatography using silica gel and subsequent elution with $CHCl_3$/MeOH/AcOH (40:1:0.1) to afford Fmoc-TEG (1.19 g, 73%). ESI-MS, *m/z*: 430 $[M+H]^+$: Found 430.

Synthesis of Fmoc-TEG-c(-Arg(Pbf)-Gly-Asp(O^{t}Bu)-D-Phe-Lys-) (2). Fmoc-TEG (0.16 g, 0.36 mmol), c(-Arg(Pbf)-Gly-Asp(O^{t}Bu)-D-Phe-Lys-) (0.3 g, 0.33 mmol) (*65*) and 1-hydroxybenzotriazole monohydrate (HOBt, 0.049 g, 0.36 mmol) were dissolved in 13 mL of dimethylformamide (DMF) and cooled to -3 °C. Subsequently, 1-ethyl-3-(3-dimethylaminopropyl)-carbodiimide·hydrochloride (EDC, 0.21 g, 1.08 mmol) in 12 mL of DMF was added dropwise during 1 h under N_2 atmosphere. The reaction mixture was further stirred for 1 h and then reacted overnight at room temperature. The solvent was removed in vacuo and then the residue dissolved in 100 mL of CH_2Cl_2 was washed with 5% citric acid (2 × 40 mL). The organic layer was collected and dried over $MgSO_4$. After removing the solvent in vacuo, the residue was purified with open column chromatography using silica gel and subsequent elution with $CHCl_3$/MeOH (20:1) to obtained compound **2** as a white solid (0.22 g, 51%). ESI-MS, *m/z*: 1345 $[M+Na]^+$: Found 1345.

Synthesis of TEG-c(-Arg(Pbf)-Gly-Asp(O^{t}Bu)-DPhe-Lys-) (3). Fmoc-TEG-c(-Arg(Pbf)-Gly-Asp(OtBu)-D-Phe-Lys-) (0.47 g, 0.35 mmol) was dissolved in 23 mL of 10% piperidine DMF solution and then stirred for 2 h. After concentrating the solvent, Et_2O was added to the solution. The white precipitate was filtrated, washed alternatively with Et_2O and n-hexane, dried

in vacuum overnight to obtain compound **3** as a yellow solid (0.30 g, 76%). ESI-MS, *m/z*: 1101 $[M+H]^+$: Found 1101.

1,4,7-Tris-(1-tert-butoxycarbonyl-3-benzyloxycarbony-propyl)-1,4,7-triazacyclononane (4) (NOTGA-^{t}Bu$_3$-Bz$_3$). (*R*/*S*) α-Bromoglutaric acid 1-tert-butyl ester 5-benzyl ester (1.3 g, 3.64 mmol) (*66*) was dissolved in 3.5 mL of acetonitrile and the solution was added dropwise to a solution of 1,4,7-triazacyclononane (0.142 g, 1.10 mmol) in 3.3 mL acetonitrile with K_2CO_3 (0.913 g, 6.62 mmol) during 2 h at 0°C under N_2. The mixture was stirred at room temperature for 24 h. The reaction mixture was filtrated and the solvent was evaporated in vacuo. The residue was dissolved in dichloromethane (15 mL) and washed with 5% $NaHCO_3$ (3 × 10 mL) and the organic layer was dried over $MgSO_4$. After removing the solvent in vacuo, the residue was purified with open column chromatography using silica gel and subsequent elution with chloroform/acetone (50:1) to afford compound **4** as yellowish oil. *RRR/SSS* (0.637 g, 69%): ^{1}H-NMR (400 MHz, $CDCl_3$), δ (ppm): 7.28–7.34 (m, 15H, Ph); 5.10 (s, 6H, CH_2–Ph); 3.09–3.13 (t, 3H, N–CH); 2.68, 2.95 (d, J = 0.03, 12H, N-CH_2-CH_2-N); 2.42–2.53 (m, 6H, CH_2–COOBz); 1.82–2.03 (m-m, 6H, N-CH-CH_2); 1.43 (s, 27H, $C(CH_3)_3$). ^{13}C-NMR (100 MHz, $CDCl_3$), δ (ppm): 173.06 (COOBzl); 173.27 (COO-^{t}Bu); 128.13, 128.17, 128.49, 136.02 (Ph); 81.80 (C-Me_3); 67.26 (C-Ph); 66.14 (N-C); 54.24 (N-C-C-N); 31.27 (C-COO-Bzl); 28.26 (^{t}Bu); 25.26 (C-COO-Bzl). *RRS/SSR* (0.165 g, 17%): ^{1}H-NMR (400 MHz, $CDCl_3$), δ (ppm): 7.27–7.34 (m, 15H, Ph); 5.10,5.09 (s-s, 6 H, CH_2–Ph); 3.09–3.14 (m, 3H, N–CH); 2.93 (d, J = 0.03, 2H, N-CH_2); 2.70–2.84 (m, 8H, N-CH_2-CH_2-N); 2.58 (d, J = 0.03, 2H, CH_2-N); 2.40–2.55 (m, 6H, CH_2-COOBz); 1.80–2.04 (m-m, 6H, N-CH-CH_2); 1.43,1.44 (s-s, 27H, $C(CH_3)_3$). ^{13}C-NMR (100MHz, $CDCl_3$), δ (ppm): 173.34, 173.45 (d, COOBzl); 172.62, 172.74 (d, COO-^{t}Bu); 128.41, 128.46, 128.77, 136.31 (Ph); 81.09, 81.11 (C-Me_3); 67.25 (C-Ph);

66.40, 66.59 (N-C); 53.85, 54.16, 54.60 (N-C-C-N); 31.33, 31.51 (C-COO-Bzl); 28.56 (^{t}Bu); 25.48, 25.65 (C-COO-Bzl). ESI-MS, *m/z*: 958 $[M+H]^+$, Found 958.

1,4,7-(α-Bromoglutaric acid 1-tert-butyl ester 5-benzyl ester)-1,4,7 triazacyclononane (5) (NOTGA-^{t}Bu$_3$). The *RRR/SSS* (0.57 g, 0.59 mmol) or *RRS/SSR* (0.15 g, 0.16 mmol) fractions were dissolved in methanol/water (5:1) and then 10% Pd/C (381 and 103 mg, respectively) was added portionwise. The mixtures were stirred for 12 h under H_2 atmosphere. Then filtered over Celite, and evaporated to dryness to obtain compound **5** as white solids. The products were used without further purification. *RRR/SSS* (408 mg, 96.4%). ^{1}H-NMR (400 MHz, CD_3OD), δ(ppm): 3.69–3.70 (br, 3H, N-CH); 2.99–3.13 (br, 12H, N-CH_2-CH_2-N); 2.52–2.64 (br, 6H, CH_2-COOH); 2.06–2.19 (br, 6H, N-CH-CH_2); 1.51 (s, 27H, $C(CH_3)_3$). *RRS/SSR* (104 mg, 95%). ^{1}H-NMR (400 MHz, CD_3OD), δ(ppm): 3.62–3.72 (br, 3H, N-CH); 2.87–3.22 (br, 12H, N-CH_2-CH_2-N); 2.44–2.81 (br, 6H, CH_2-COOH); 2.19–2.15 (br, 6H, N-CH-CH_2); 1.51 (s, 27H, $C(CH_3)_3$). ESI-MS, *m/z*: 688 $[M+H]^+$, Found 688.

NOTGA-(TEG-RGD)$_3$ (6). NOTGA-^{t}Bu$_3$ (*RRR/SSS*, 8.52 mg, 12.4 μmol; *RRS/SSR*, 10 mg, 14.5 μmol) was dissolved in dry CH_2Cl_2 (0.5 mL) and 0.3 eq of 4-dimethylaminopyridine (DMAP), 3.5 eq of TEG-c(-Arg(Pbf)-Gly-Asp(O^{t}Bu)-D-Phe-Lys-), 3.6 eq of EDC dissolved in 0.5 mL of CH_2Cl_2 were added dropwise on an ice bath. After stirring at room temperature for 12 h under N_2, the solvent was evaporated in vacuo. The residue was dissolved in CH_2Cl_2 (10 mL), washed with 5% $NaHCO_3$ (3 × 7 mL) and dried over $MgSO_4$. After removing the solvent, the residue was taken up by a small amount of $CHCl_3$. The precipitate formed upon addition of excess of Et_2O was filtrated and dried in vacuum overnight to obtain the protected conjugate intermediate as a yellow solid (*RRR/SSS*, 33.3 mg, 68.2%; *RRS/SSR*, 38.7 mg, 67.6%). ESI-MS, m/z: 1683.9 $[M+2H]^{2+}$: Found 1685.5. After treatment with TFA/triethylsilane/H_2O (90:5:5) at

room temperature for 3 h, the solvent was evaporated in vacuo and the precipitate formed upon addition of excess of Et_2O (*RRR/SSS*, 17.8 mg, 64.6%; *RRS/SSR*, 16 mg, 57.1%). ESI-MS, *m/z*: 1422 $[M+2H]^{2+}$: Found 1422.

Ga-NOTGA-(TEG-RGD)$_3$. NOTGA-(TEG-RGD)$_3$ (*RRR/SSS*, 0.8 mg, 0.28 μmol; *RRS/SSR*, 3 mg, 1.05 μmol) was dissolved in 500 μL of water, and 0.1 M $Ga(NO_3)_3$ solution (4.4 and 14.3 μL, respectively) were added. After 10 min heating at 70°C, the pH was adjusted from 1.9 to 3.5 using 1 M sodium acetate and heated for another 30 min. The complex was purified by preparative HPLC and lyophilized to obtain Ga-NOTGA-(TEG-RGD)$_3$ (*RRR/SSS*, 0.7 mg, 85%; *RRS/SSR*, 2.67 mg, 87%). ESI-MS, m/z: 1455 $[M+2H]^{2+}$, Found 1455.

2.2.3. ^{67}Ga-Radiolabeling

The complexation of ^{67}Ga by both diasteremeric pair of ligands was studied regarding the reaction pH and time at room temperature. $^{67}GaCl_3$ (10 μL, 1.5 MBq) in 0.05 M HCl was mixed with 10 μL of 0.5 M sodium acetate buffer (A.B.) pH 4 – 5.5. The mixtures were added to Eppendorf tubes containing 0.4 nmol of ligand in 20 μL of 0.25 M acetate buffer pH 3 – 5.5 to give final solutions of 0.25 M A.B., pH 3.5 – 5.5 and 10 μM of ligand concentration. The mixtures were incubated at 25ºC for 5, 10 and 15 min and radiochemical yield were determined by Radio-TLC.

2.2.4. In vitro stability

^{67}Ga labeled complexes (*RRR/SSS, RRS/SSR*) were purified by RP-HPLC to remove unlabeled ligands. The radioactive peak was collected and the solvent was removed in vacuo. The residue was reconstituted in apo-Tf solution (50 μM, 0.1 M carbonate buffer, pH 7.4) and

incubated at 37°C. Samples were withdrawn at 1, 3 and 6 h and analyzed by Radio-TLC (n = 3).

2.2.5. Binding affinity to integrin $\alpha_v\beta_3$

To evaluate the binding affinity of Ga labeled compounds to integrin $\alpha_v\beta_3$, surface plasmon resonance (SPR) technology-based ProteOn™ XPR36 protein interaction array system (Biorad Laboratories Japan, Yokohama, Japan) was used. The SPR experiment was performed according to the manufacturer's instruction. In brief, human purified integrin $\alpha_v\beta_3$ (20 μg/mL, Chemicon International, Temecula, CA, USA) dissolved in 10 mM A.B. (pH 4.0) was immobilized on a ProteOn GLH sensor chip (Biorad Laboratories Japan) by standard amine coupling method. The Ga-NOTGA-(TEG-RGD)$_3$ complexes (*RRR/SSS*, *RRS/SSR*) at 10, 5, 2.5 and 1.25 μM concentrations and c(RGDfk) at 200, 100, 50, 25 and 12.5 μM as a positive control in 10 mM Tris-HCl buffer (50 mM NaCl, 1 mM $MgCl_2$, 1 mM $MnCl_2$, pH 7.4) were injected simultaneously into the six horizontal channels of the chip. Kinetic analysis was performed by globally fitting curves describing a simple 1:1 biomolecular model to the set of five sensorgrams.

2.2.6. Cell line

Human glioblastoma U87MG cells were grown in a 75 cm^2 tissue culture flask with canted neck (Becton, Dickinson and Company, Tokyo) in Dulbecco's Modified Eagle Medium (Sigma-Aldrich Japan K.K., Tokyo) supplemented with 10% fetal calf serum (FCS, Nippon Bio-supply Center, Tokyo) and GIBCO BRL 1% penicillin–streptomycin (5000 unit – 5000 μg/mL, Invitrogen, Life Technologies Japan Ltd., Tokyo), at 37°C in a humidified atmosphere containing 5% CO_2.

2.2.7. Biodistribution studies

Animal studies were conducted in accordance with institutional guidelines approved by the Chiba University Animal Care Committee. Male ddY mice (*67*) (Japan SLC, Inc., Shizuoka, Japan) of 6-week-old were injected via tail vein with either *RRR/SSS* or *RRS/SSR* diastereomers of ^{67}Ga-NOTGA-(TEG-RGD)$_3$ (100 μL, 11.1 KBq, 10 μM ligand concentration). The animals were sacrificed and dissected at 30 min, 1 h, 3 h and 6 h after administration. Tissues of interest were removed, weighted and the radioactivity counts were determined with an auto well gamma counter. The urine and feces were collected for 6 h and the radioactivity was also measured. Values were expressed as mean ± SD for a group of 3 – 5 animals.

BALBc nu/nu male mice (Japan SLC, Inc, Shizuoka, Japan) of 6-week-old, 18 – 20 g, were xenografted by subcutaneous (s.c.) injection of U87MG human glioblastoma cells (5×10^6 cells/80 μL of culture medium) into their right hind legs. The mice were subjected to biodistribution studies as well as SPECT/CT imaging studies when the tumor volume reached 100 – 300 mm^3.

Biodistribution studies were also conducted in male BALBc nu/nu mice bearing U87MG xenografts 30 min after administration of each radiotracer (n = 4). The integrin $\alpha_v\beta_3$ specificity was estimated by co-injection of either *RRR/SSS* or *RRS/SSR* diastereomers of ^{67}Ga-NOTGA-(TEG-RGD)$_3$ (100 μL, 11.1 KBq, 10 μM ligand concentration) and c(RGDyV) peptide (3 mg/kg mouse body weight) into mice bearing U87MG tumors. The animals were sacrificed and dissected at 2 h after administration (n = 4).

2.2.8. Small Animal SPECT/CT imaging studies

SPECT/CT images were taken 30 min after administration of either *RRR/SSS* or *RRS/SSR* diastereomers of [^{67}Ga]-NOTGA-(TEG-RGD)$_3$ (100 μL, 4.5 MBq, 10 μM ligand concentration) to male BALBc nu/nu mice bearing U87MG xenografts from the tail vein (n = 3). The mice were anaesthetized with 1 – 2% (v/v) isoflurane (DS Pharma Animal Health, Osaka, Japan) and positioned on the animal bed where anesthesia was continuously delivered via a nose cone system. SPECT imaging and X-ray CT imaging were performed by use of small animal SPECT/CT system (FX-3200, Gamma Medica Inc., CA) equipped with five pinholes (0.5 mm) collimator. Data acquisition was performed for 64 min at 60 s per projection with stepwise rotation of 64 projections over 360˚.

2.2.9. Statistical analysis

Quantitative data were expressed as mean ± SD. Means were compared using unpaired two-tailed Student's t test. P values <0.05 were considered statistically significant.

2.3. Results

2.3.1. Chemical synthesis

TACN was alkylated with (*R/S*) α-bromoglutaric acid 1-tert-butyl ester 5-benzyl ester (*15, 66, 68*) in acetonitrile and K_2CO_3 at room temperature to obtain the fully protected NOTGA-^{t}Bu$_3$-Bz$_3$ **4** (Scheme 2.1). Purification was carried out using silica-gel column chromatography and a mixture of chloroform and acetone as the mobile phase. Two fractions (a major fraction of 69% and the following of 17%) were verified to be the target compound by mass spectrometry.

Structure assignment was possible by ^{1}H-NMR and ^{13}C-NMR, which provides deeper insights into their structural differences (Figure 2.3 – 2.5). Focusing on the chiral carbon (label b in Figure 2.3), a single resonance was observed in the 69% fraction Figure 2.3 A) indicating equivalent carbons, and two resonances in the 17% fraction indicating the presence of two chemically non-equivalent carbons (Figure 2.3 B). The 69% fraction was assigned to the *RRR*/*SSS* diastereomeric pair and the 17% to the *RRS*/*SSR*.

In order to evaluate the differences of both diastereomeric pairs, each fraction was treated separately. After debenzylation by palladium catalyzed hydrogenolysis, the diastereomeric orthogonally protected NOTGA-^{t}Bu$_3$ prochelators were obtained in quantitative yields.

The peptide substituent was prepared using an Fmoc chemistry to introduce the TEG spacer in the lysine side chain of c(RGDfK) in 50 % yield. The prochelators of NOTGA-^{t}Bu$_3$ were then conjugated to the partially protected TEG-c(-Arg(Pbf)-Gly-Asp(O^{t}Bu)-D-Phe-Lys-) by in situ activation using the standard EDC based coupling method followed by complete removal of all protecting groups to obtain the desired ligands at moderate yields after HPLC purification (> 95% purity).

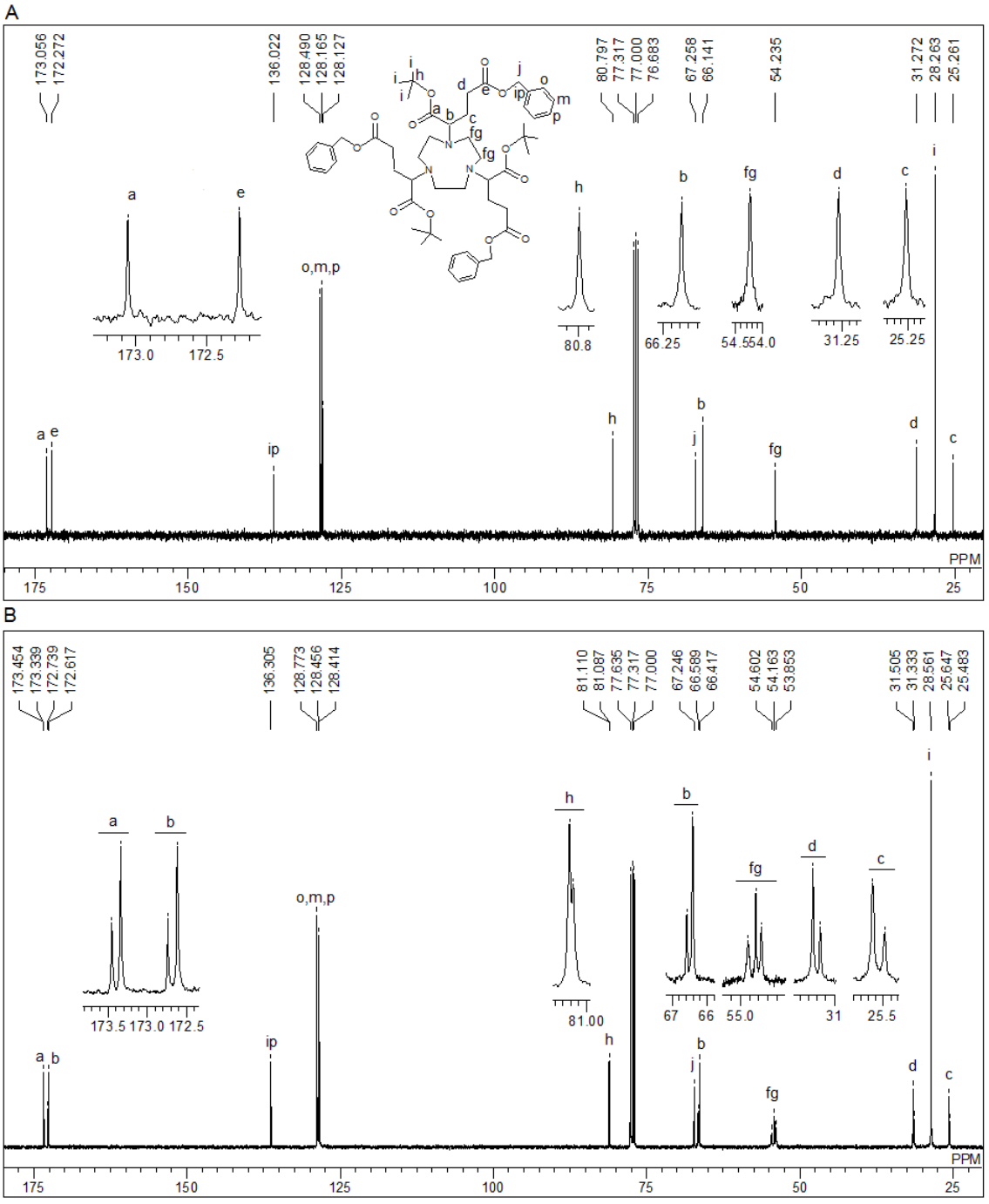

Figure 2.3. ^{13}C NMR (100MHz, $CDCl_3$, 25 °C) spectra of NOTGA-$^{t}Bu_3$-Bz_3 products obtained from alkylation of TACN with (*R*/*S*)-α-bromoglutaric acid 1-tert-butyl ester 5-benzyl ester, followed by column chromatography. (A) The major fraction (69 %) corresponds to *RRR/SSS* enantiomers while (B) the minor fraction (17 %) to *RRS/SSR* diastereomers. See inserted structural formula for assignments

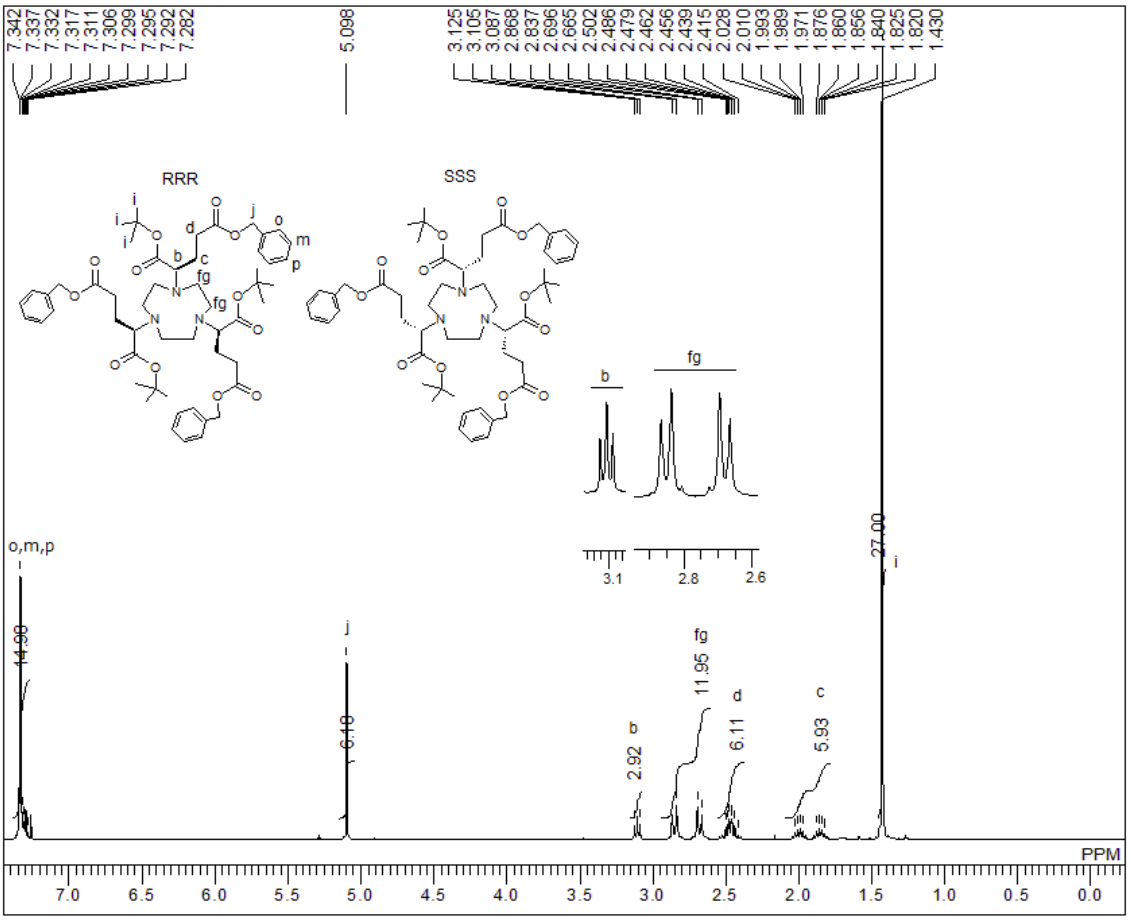

Figure 2.4. ^{1}H NMR (400 MHz, $CDCl_3$, 25 °C) spectra of NOTGA-$^{t}Bu_3$-Bz_3 from the alkylation of TACN with (*R*/*S*)-α-bromoglutaric acid 1-tert-butyl ester 5-benzyl ester. Column chromatography isolated fraction (69%) corresponding to *RRR/SSS* enantiomers. See inserted structural formulas for assignments

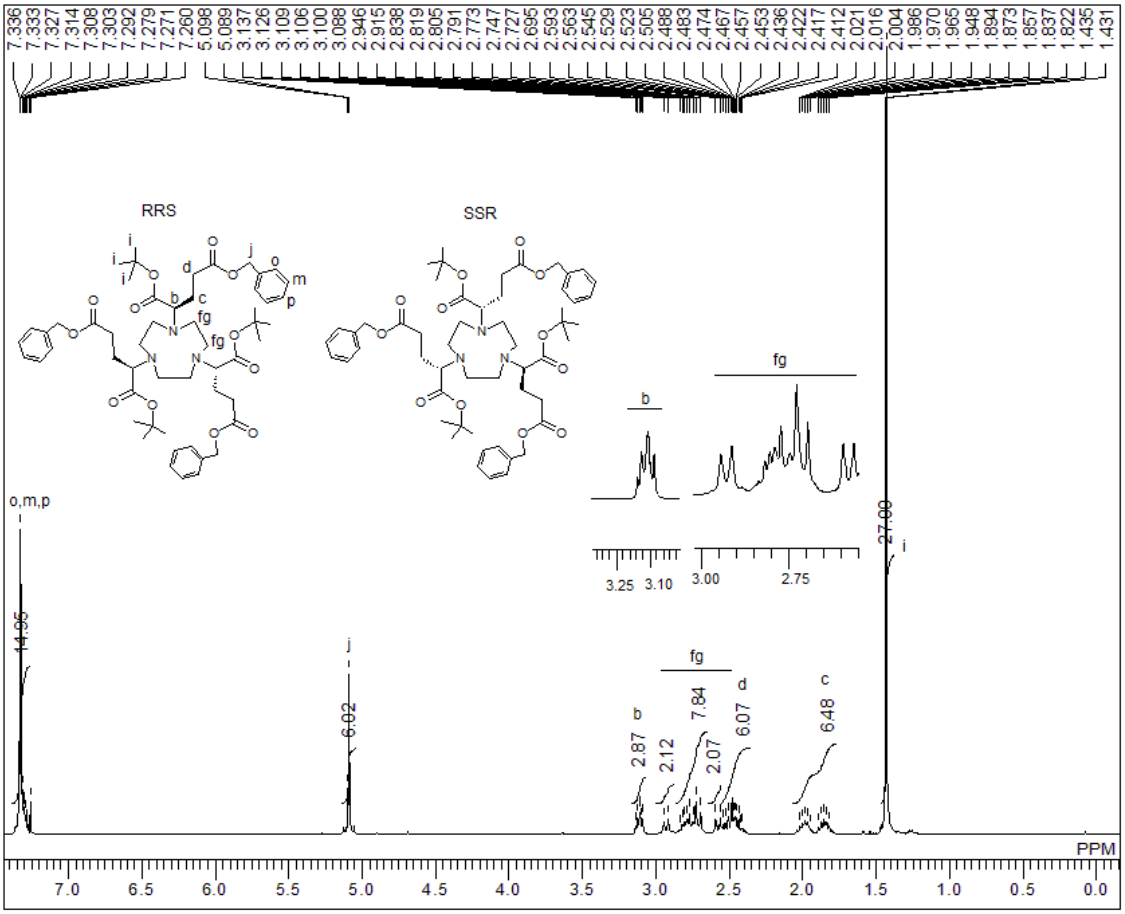

Figure 2.5. ^{1}H NMR (400MHz, $CDCl_3$, 25 °C) spectra of NOTGA-$^{t}Bu_3$-Bz_3 from the alkylation of TACN with (*R/S*)-α-bromoglutaric acid 1-tert-butyl ester 5-benzyl ester. Column chromatography isolated fraction (17%) corresponding to the *RRS/SSR* diastereomers. See inserted structural formulas for assignments

2.3.2. Radiochemistry

The *RRR*/*SSS* and *RRS*/*SSR* pairs of NOTGA-(TEG-RGD)$_3$ were radiolabeled with ^{67}Ga and the resulting complexes were analyzed by HPLC (Figure 2.6). In both cases, a single peak was observed and the retention time of the *RRR*/*SSS* was 24.5 min, slightly longer than that of *RRS*/*SSR* (24.3 min). In both cases, their retention times were identical to those of the corresponding non-radioactive gallium complexes verified by mass spectrometry.

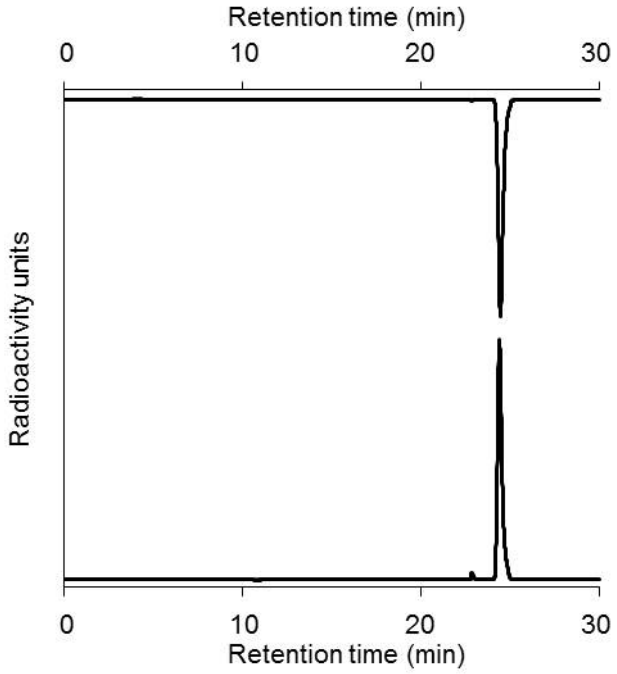

Figure 2.6. HPLC radiochromatograms of ^{67}Ga-NOTGA-(TEG-RGD)$_3$. The *RRR*/*SSS* diastereomer (top) was eluted at 24.5 min slightly longer than that of the *RRS*/*SSR* counterpart (bottom, 24.3 min)

Formation kinetic as a function of pH is presented in Figure 2.7. In both cases, radiochemical yields were low under acidic conditions (pH 3.5) and quantitative at higher pH. Interestingly, while *RRR*/*SSS* was preferentially labeled at pH 5 the *RRS*/*SSR* was pH independent from pH 4 to 5.5 (Figure 2.7 A). Nevertheless, at pH 5 the time variation of the radiochemical yield was essentially the same for both pairs (Figure 2.7 B) and complete radiolabeling with more than 98% yield was attained after 10 min of reaction. Under the present conditions, the specific activity of the ^{67}Ga-labeled compounds was 4,500 MBq/µmol.

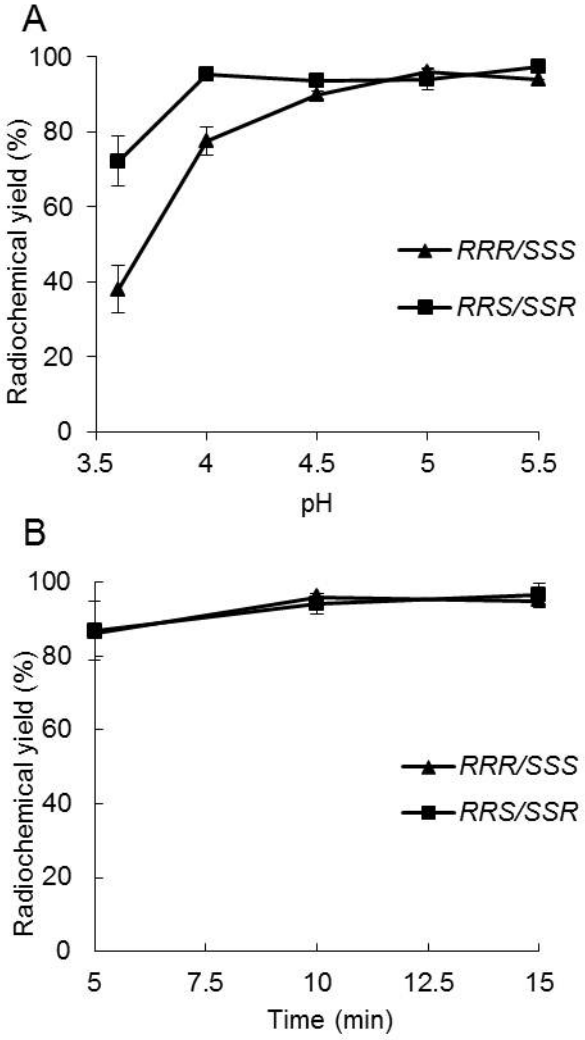

Figure 2.7. Radiochemical yields of each diastereomer of ^{67}Ga-NOTGA-(TEG-RGD)$_3$ (*RRR*/*SSS*: squares, and *RRS*/*SSR*: triangles) (A) at different pH values for 10 min and (B) different reaction times at pH 5.0

2.3.3.In vitro stability

The kinetic stability of [^{67}Ga]-NOTGA-(TEG-RGD)$_3$ diastereomeric pairs, purified by HPLC in order to remove the excess of ligand, was estimated in an apo-Tf challenge (Table 2.1). After 6 h of incubation at 37°C, more than 98% of the radioactivity was still bound to the NOTGA tri-peptide conjugates of both pairs.

Table 2.1. Stability of ^{67}Ga-NOTGA-(TEG-RGD)$_3$ diastereomers against apo-Tf[a]

Time (h)	Percent of intact radiolabeled complex	
	RRR/SSS	***RRS/SSR***
1	98.6 ± 0.2	98.9 ± 0.4
3	98.9 ± 0.3	98.3 ± 0.9
6	98.0 ± 0.4	98.4 ± 0.2

[a]Results are expressed as mean ± SD of three experiments

2.3.4. Binding affinity

The binding kinetics of the two diasteromeric gallium complexes of NOTGA-(TEG-RGD)$_3$ to $\alpha_v\beta_3$ integrin was estimated with the SPR technology using a monovalent c(RGDfK) as a reference (Table 2.2). Both diastereomeric trivalent complexes exhibited higher association and lower dissociation rates than that of a monovalent c(RGDfK) with the rate constants similar each other. As a result, both trivalent complexes showed 10-folder lower dissociation constant values (K_D) than that of monovalent c(RGDfK).

Table 2.2. Kinetic binding constants of ^{67}Ga-NOTGA-(TEG-RGD)$_3$ (*RRR/SSS* and *RRS/SSR*), c(RGDfK) to integrin $\alpha_v\beta_3$ determined using the SPR technology

Analyte	K_a (1/Ms)	K_d (1/s)	K_D(M)
RRR/SSS	$1.13 \times 10^5 \pm 6.8 \times 10^3$	$8.03 \times 10^{-3} \pm 1.7 \times 10^{-4}$	$7.13 \times 10^{-8} \pm 4.5 \times 10^{-9}$
RRS/SSR	$0.94 \times 10^5 \pm 5.3 \times 10^3$	$8.12 \times 10^{-3} \pm 1.6 \times 10^{-4}$	$8.64 \times 10^{-8} \pm 4.9 \times 10^{-9}$
c(RGDfK)	$2.57 \times 10^4 \pm 6.1 \times 10^3$	$1.38 \times 10^{-2} \pm 6.2 \times 10^{-4}$	$5.37 \times 10^{-7} \pm 2.7 \times 10^{-7}$

2.3.5. In vivo experiments

The results of the biodistribution studies of [^{67}Ga]-NOTGA-(TEG-RGD)$_3$ in normal mice at

30 min, 1 h, 3 h and 6 h after administration are shown in Table 2.3 (*RRR/SSS*) and Table 2.4 (*RRS*/*SSR*). No significant differences were observed in the uptake of both diastereomers in almost all organs and tissues. These profiles were characterized by rapid blood clearance with low accumulation in the liver and the majority of the radioactivity was localized in the kidneys.

Table 2.3. Biodistribution of *RRR/SSS* diastereomer of ^{67}Ga-NOTGA-(TEG-RGD)$_3$ in normal mice[a]

	RRR/SSS			
Organ	**30 min**	**1 h**	**3 h**	**6 h**
Blood	0.61 ± 0.13	0.16 ± 0.02	0.07 ± 0.02	0.09 ± 0.02
Liver	1.27 ± 0.22	1.32 ± 0.15	1.49 ± 0.32	1.50 ± 0.30
Spleen	2.09 ± 0.35	1.26 ± 0.12	1.32 ± 0.21	1.77 ± 0.56
Kidneys	5.82 ± 1.22	5.04 ± 1.15	3.48 ± 0.54	3.00 ± 0.43
Pancreas	1.06 ± 0.19	0.72 ± 0.09	0.65 ± 0.10	0.66 ± 0.13
Heart[b]	1.00 ± 0.07	0.69 ± 0.05	0.65 ± 0.09	0.73 ± 0.11*
Lung	2.52 ± 0.33	1.41 ± 0.11	1.08 ± 0.37	1.25 ± 0.47
Muscle	0.84 ± 0.14	0.55 ± 0.12	0.51 ± 0.07	0.52 ± 0.04
Stomach[c]	0.63 ± 0.06	0.74 ± 0.16	0.56 ± 0.13	0.47 ± 0.14
Intestines[b,c]	2.98 ± 0.54	3.67 ± 0.27**	5.23 ± 0.80*	4.44 ± 0.26**
Urine[c]				63.22 ± 6.83
Feces[c]				4.25 ± 1.30

[a]Data expressed as %ID/g ± SD (n = 5). [b]* $p < 0.05$, ** $p < 0.01$ in comparison to *RRS/SSR*. [c]Expressed as %ID

Both radioligands were excreted in the urine with a small amount in feces. Although in absolute terms the uptake in the intestines was very low, a slight tendency of the *RRR/SSS* to be excreted through the intestinal tract can be noted. Its intestine accumulation was significantly higher at 1, 3 and 6 h p.i. Likewise, relatively higher radioactivity in feces and lower radioactivity in urine for the *RRR*/*SSS* were observed.

Table 2.4. Biodistribution of *RRS/SSR* diastereomer of ^{67}Ga-NOTGA-(TEG-RGD)$_3$ in normal mice[a]

	RRS/SSR			
Organ	**30 min**	**1 h**	**3 h**	**6 h**
Blood	0.58 ± 0.18	0.19 ± 0.02	0.09 ± 0.03	0.08 ± 0.02
Liver	1.22 ± 0.12	1.19 ± 0.07	1.56 ± 0.38	1.33 ± 0.19
Spleen	1.42 ± 0.59	1.20 ± 0.17	1.40 ± 0.06	1.57 ± 1.17
Kidneys	5.38 ± 0.89	4.74 ± 0.87	3.58 ± 0.39	3.04 ± 0.28
Pancreas	0.85 ± 0.07	0.69 ± 0.03	0.71 ± 0.09	0.58 ± 0.11
Heart[b]	0.93 ± 0.16	0.73 ± 0.08	0.73 ± 0.09	0.55 ± 0.05*
Lung	1.94 ± 0.53	1.36 ± 0.16	1.33 ± 0.35	1.00 ± 0.04
Muscle	1.22 ± 0.91	0.55 ± 0.04	0.55 ± 0.06	0.62 ± 0.17
Stomach[b]	0.59 ± 0.06	0.63 ± 0.11	0.61 ± 0.11	0.40 ± 0.02
Intestines[b]	2.59 ± 0.35	3.00 ± 0.27**	4.10 ± 0.62*	2.90 ± 0.38**
Urine[b]				71.52 ± 2.64
Feces[b]				2.24 ± 0.89

[a]Data expressed as %ID/g ± SD (n = 5). [b]Expressed as %ID

Figure 2.8 shows the biodistribution studies of [^{67}Ga]-NOTGA-(TEG-RGD)$_3$ (*RRR*/*SSS* and *RRS*/*SSS*) at 30 min postinjection to nude mice bearing U87MG xenografts. The biodistribution profiles of both diastereomeric pairs were characterized by rapid blood clearance, high tumor uptake with comparatively low accumulation in non-target organs and renal excretion pathway. In agreement with the studies in normal mice, the uptakes of the diastereomeric pairs in organs of interest were comparable. Tumor uptakes were 4.40 ± 0.38 and 4.77 ± 0.76 %ID/g (p<0.05) for *RRR*/*SSS* and *RRS*/*SSR*, respectively. Tumor to organ ratios (Figure 2.8 B) were high for blood and muscle, moderate for the liver and much lower for the kidney. A combination of slightly higher tumor and lower blood uptakes led to a statistically significantly higher tumor to blood ratio for the *RRS*/*SSR* pair.

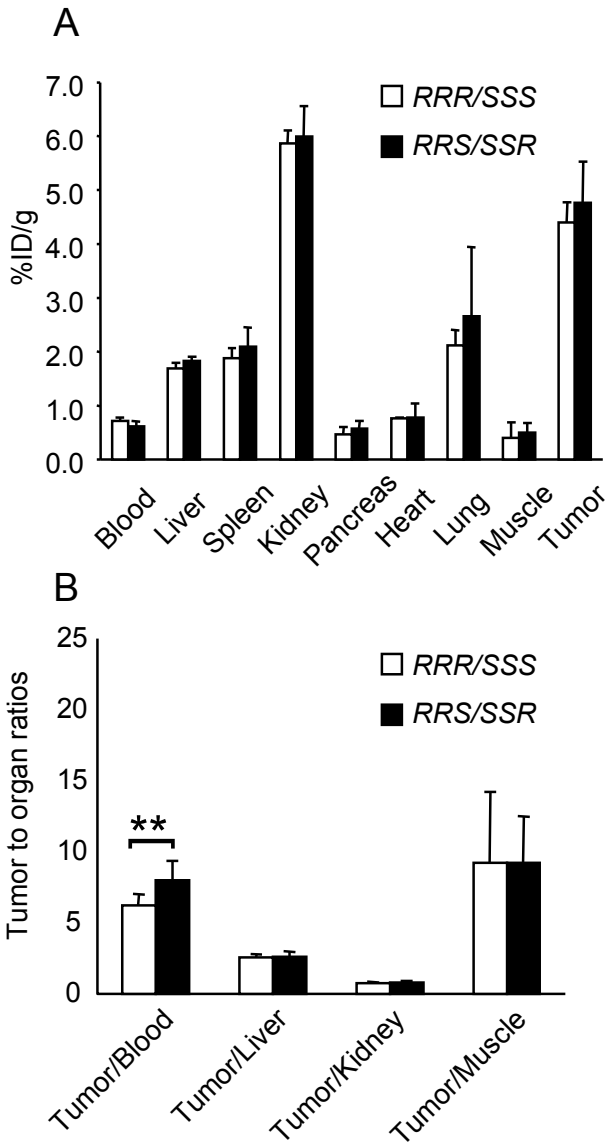

Figure 2.8. (A) Biodistribution of ^{67}Ga-NOTGA-(TEG-RGD)$_3$ in tumor-bearing male nude mice at 30 min after intravenous injection of 11.1 KBq of *RRR/SSS* (white) or *RRS/SSR* (black). (B) The tumor to organ ratios of the ^{67}Ga labeled conjugates. Data expressed as %ID/g ± SD ($n = 4$, ** $p < 0.01$)

When the radiolabeled probes were co-injected with a high amount of RGDyV, tumor accumulation was significantly decreased ($p < 0.05$) to 0.82 ± 0.17 and 0.68 ± 0.2 %ID/g at 2 h p.i. (*RRR*/*SSS* and *RRS*/*SSR*, respectively), demonstrating integrin $\alpha_v\beta_3$ targeting specificity (Figure 2.9).

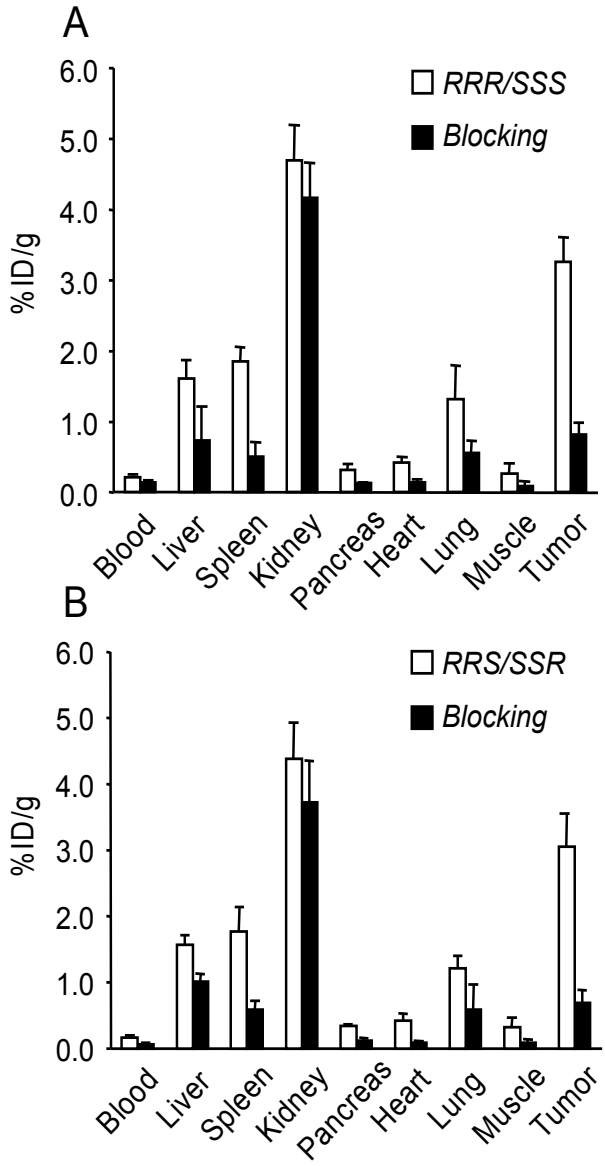

Figure 2.9. Biodistribution data in tumor-bearing male nude mice at 2 h after administration of ^{67}Ga-NOTGA-(TEG-RGD)$_3$ with (black) and without (white) the presence of an excess of RGDyV. (A) *RRR/SSS;* (B) *RRS/SSR*. Data expressed as %ID/g ± SD (n = 4)

SPECT/CT imaging studies were performed for both *RRR*/*SSS* and *RRS*/*SSS* diastereomers of [^{67}Ga]-NOTGA-(TEG-RGD)$_3$ using nude mice bearing U87MG xenografts (Figure 2.10). Tumors were clearly visualized as early as 30 min after administration. Radioactivity was concentrated in the kidneys and bladder. Impressively, non-specific accumulation in liver or

bowel was not observed resulting in high contrast images.

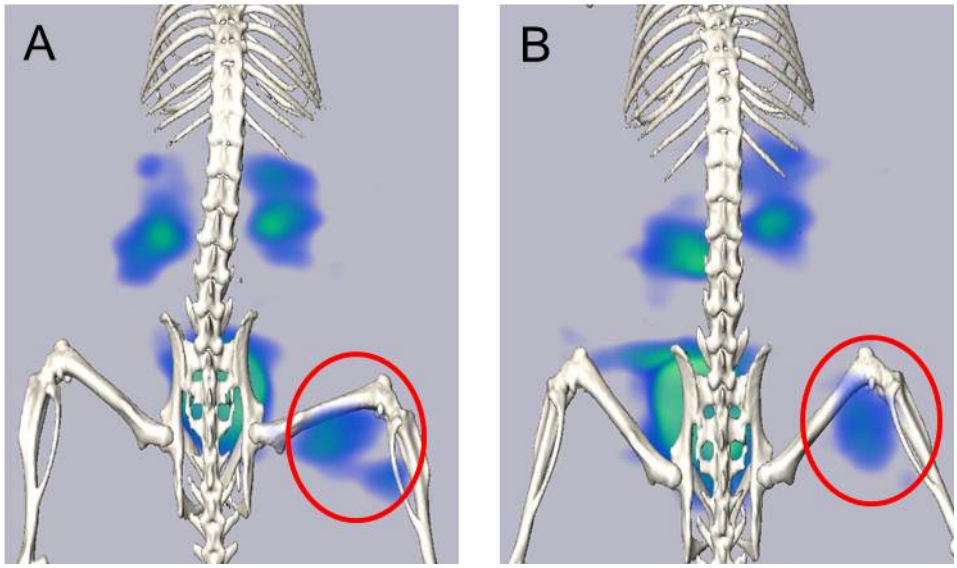

Figure 2.10. SPECT/CT images of U87MG tumor-bearing male nude mice after 30 min of i.v. injection of 4.5 MBq of each diastereomer of [^{67}Ga]-NOTGA-(TEG-RGD)$_3$. (A) *RRR*/*SSS* and (B) *RRS*/*SSR*. Images were shown at the same signal intensity scale

2.4. Discussion

The cyclic RGD peptides have been widely study as a targeting molecule due to its high affinity for integrin $\alpha_v\beta_3$ over-expressed during tumor angiogenesis.(*11*) It has also been well recognized that in vitro binding affinity and in vivo tumor targeting ability of multimeric RGD peptides are enhanced due to the multivalent effect and the enriched local RGD concentration.(*11, 18-21*) Moreover, it has been demonstrated that the spacer units of appropriate length and hydrophilicity between a radiometal chelate and each RGD motif increase avidity of the radiotracers and simultaneously may act as pharmacokinetic modifier to improve pharmacokinetics of the radiotracer.(*11, 69, 70*)

The preparation of NOTA-based radiopharmaceuticals was conducted according to the

procedure reported previously.(*16, 17*) In brief, the synthesis of the orthogonally protected prochelator NOTGA-^{t}Bu$_3$ took place first, followed by conjugation of the bioactive molecules to each carboxylic acid of the pendant arm and final deprotection. Intermediate **4** exists in different isomeric forms,(*60, 61*) *RRR*, *SSS*, *RRS*, and *SSR* (Figure 2.2) due to the use of the (*R*/*S*) racemates of α-bromoglutaric acid 1-tert-butyl ester 5-benzyl in the alkylation of TACN. They were synthesized from (*S*)-glutamic acid-5-benzyl ester through bromination by diazotization with sodium nitrite in NaBr/HBr solution as previously.(*15, 17, 60, 66*) This reaction is not stereoselective and the α-bromo acid product is only enantioenriched as reported.(*71*) Further methods should be devised at this stage to isolate the major fraction by chiral chromatography or by using enantioselective bromination reactions.(*72*) The *RRR* and *SSS* isomers constitute enantiomers with three equivalent chiral carbons and the pair was assigned to the 69% fraction with a single resonance at the corresponding position in ^{13}C-NMR. Enantioenriched reactants may have favored the formation of this two enantiomers. Likewise, two different carbons (*R*, *S*) are present in *RRS*/*SSR* and were associated with the two resonances observed in the 17% fraction. A similar phenomena was observed in the tetralkylation of the tetraazacyclodecane analogue with racemix α-bromo acid diesters.(*61*)

It should be mention that besides the isomerism in NOTGA ligands coming from the chiral carbon in the pendant arms, NOTA-based complexes are chiral depending on the orientation of the pendant arms around the metal center (Λ: clockwise or Δ: anticlockwise) and the relative puckering of the ethylenediamine subunit chelate rings (δδδ or λλλ conformers).(*73, 74*) In case of gallium, only the enantiomeric Δ(λλλ)/Λ(δδδ) combination has been observed.(*73*) Therefore, each *RRR/SSS* and *RRS/SSR* of Ga-NOTGA diastereomeric pair may further exist as the enantiomeric combinations Δ(λλλ)-*RRR*/Λ(δδδ)-*SSS* or Δ(λλλ)-*SSS*/Λ(δδδ)-*RRR*), as well as, Δ(λλλ)-*RRS*/Λ(δδδ)-*SSR* or Δ(λλλ)-*SSR*/Λ(δδδ)-*RRS*. Further, X-ray crystallography analysis

or computational modeling methods would clarify the actual structure. Nevertheless, both diastereomeric ligands provided gallium complexes of high inertness, demonstrated in the apo-Tf challenge, indicating good retention of the metal inside the complex cavity.

^{67}Ga radiolabeling was performed at room temperature as previously reported for NOTA and its derivatives.(*13, 56, 57*) The reaction condition allowed assessing the differences in the complexation ability of the diastereomeric ligands that otherwise would be suppressed by heating. Lower radiochemical yields under acidic conditions were also found by Singh et al. (*17*) when labeling NOTGA and its di-substituted parent, in comparison to the mono-substituted and the *p*-SCN-Bn-NOTA RGD conjugates, possibly due to steric hindrance caused by the three substituents. On the other hand, pH 5 was found optimal for labeling NODAGA-RGD with ^{68}Ga,(*75*) and a study of the Ga-NOTA formation in acetate solutions found faster reaction rates at higher pH.(*76*) Intriguingly, the *RRS*/*SSR* was almost pH-independent from pH 4 to 5.5. A hypothesis to account for this observation would be related to the formation mechanism of the Ga-NOTA complex and the structural differences between the diastereomers.

It has been reported that complexation of NOTA and other polyazamycrocycles containing pendant arms proceed in two steps. The first step comprises a fast formation of a monoprotonated intermediate species in which the metal ion is outside of the macrocyclic cage and coordinated to the three peripheric carboxylate oxygen atoms. The ring nitrogen atoms remain unbound and the proton would be attached to one of them. In the second step, deprotonation takes place followed by migration of the metal to inside the cavity where it also becomes coordinated to the nitrogen atoms.(*77*) Due to electrostatic repulsion between the nitrogen's proton and the metal, removal of the proton is considered to be the rate-determining step. (*76, 78, 79*) It has been proposed this is an OH-catalyzed deprotonation,(*76-79*) explaining

the faster complexation at higher pH. It has also been proposed that the migration of the proton from the NH^+ group to a carboxylate facilitates the accessibility with respect to OH^- ions.(*79*) In either cases, the *RRS/SSR* conformation might facilitate the access of the OH^- ions to the nitrogen bound proton or the proton migration to the carboxylate, making the complexation less pH dependent.

To further estimate the differences between the two diastereomers, the binding affinity of the two gallium complexes of NOTGA-(TEG-RGD)$_3$ to $\alpha_v\beta_3$ integrin were estimated by SPR assay and it was found that the structural differences in the NOTGA diastereomers presented here do not affect the interaction with the targets (Table 2.2). The binding to $\alpha_v\beta_3$ integrin is strongly dependent on the molecular design of multimeric RGD probes. There are two factors underneath the enhanced target affinity: enhanced local RGD concentration and multivalency. Although the local concentration factor is innate in all multimeric probes, an appropriate distance between each two sets of cyclic RGD motifs is required to achieve multivalency.(*11, 80, 81*) In this design, the triethylene glycol spacer was inserted to provide a distance between the RGD motifs of 37 bonds. According to the previous study,(*80*) the distance between the two cyclic RGD motifs of [^{67}Ga]-NOTGA-(TEG-RGD)$_3$ would be suitable for simultaneous $\alpha_v\beta_3$ integrin binding. In addition, Syngh et al. reported that a trimeric RGD linked to NOTGA showed enhanced tumor uptake and retention compared with monomeric RGD counterpart, due to the multivalent effect partially.(*17*) From these findings, a combination of multivalency and enhanced local RGD concentration might be attributable to higher targeting capabilities of [^{67}Ga]-NOTGA-(TEG-RGD)$_3$, reflected in a binding affinity 10 folder higher than the monovalent cRGDfK. Thus, both diastereomers might act as trivalent compounds and the spatial arrangement of the RGD motifs in each complex would be equivalent with respect to binding affinity to $\alpha_v\beta_3$ integrin.

No significant differences were also observed in the biodistribution of the ^{67}Ga labeled diastereomers (Tables 2.3 and 2.4, Figure 2.8). Both exhibited rapid blood clearance and renal excretion in normal and nude mice bearing U87MG tumors. The high renal uptake was consistent with previous studies of other multimeric RGD peptides.(*17, 19, 82-84*) It was reported that endothelial cells of the glomeruli vessels in the kidneys express integrin $\alpha_v\beta_3$,(*85*) which could partially explain the observation. The presence of three guanidine groups in the trivalent RGD conjugate would increase positive charge, which may have facilitated reabsorption in proximal renal tubular cells.(*19, 20, 85, 86*) While both diastereomers exhibited similar biodistribution, the elution order of the diastereomers from HPLC (Figure 2.6; *RRS/SSR* followed by *RRR/SSS*) suggests that a small difference in the lipophilicity between the two may be responsible for the slight tendency of the *RRR/SSS* to be excreted through the intestinal tract, though the excretion route is minimal. The similar affinity for integrin $\alpha_v\beta_3$ along with similar pharmacokinetics of the diastereomers resulted in similar tumor accumulation of the two compounds (Figure 2.8), yielding SPECT/CT images of high contrast as shown in Figure 2.10.

The longer-lived ^{67}Ga was used throughout the study. The outcomes of this study would also be applicable to the synthesis of ^{68}Ga labeled NOTGA-(TEG-RGD)$_3$. Moreover, given the efforts in the processing of generator eluates to reduce metal impurities (*1, 10, 56, 87*) and the sensitivity of PET imaging techniques, superior images of in vivo integrin $\alpha_v\beta_3$ expression can be obtained. Furthermore, NOTGA can be used also for applications with other metal radionuclides such as ^{64}Cu, which have been previously incorporated to other NOTA-based BFC.(*88*)

2.5. Conclusions

The findings in this study show that the RGD conjugates of both diastereomers presented here possess equivalent biological efficacy, and the combined usage of the diastereomic mixture would be feasible as far as the present compounds are concerned. It is worth noting that the specific properties of a given biomolecule, cell expression levels of the corresponding target molecule, presence or absence of pharmacokinetic modifiers might affect the structural differences between diastereomers on the ligand-receptor interactions and biodistribution. Since the synthesis of diastereomerically pure NOTGA-^{t}Bu prochelators has been established, the preparation of corresponding conjugates and evaluation of their chemical and biological performances still remains important for applying NOTGA to other biomolecules of interest.

Chapter 3.

General conclusions

Molecular imaging offers the potential to image non-invasively promising molecular targets; shifting the place we look for diseases from tissues and organs to molecular structures and mechanisms at cellular and subcellular levels. These molecular targets or more precisely, the corresponding targeting molecules need to be part of successful molecular probes to have a practical meaning. The outcomes of this thesis, the availability of the positron emitter zinc-63 and diastereomerically pure molecular designs for ^{68}Ga probes, will undoubtedly contribute to the development of novel PET based radiopharmaceuticals for molecular imaging.

Bibliography

(1) Tolmachev, V., and Stone-Elander, S. (2010) Radiolabelled proteins for positron emission tomography: Pros and cons of labelling methods. *Biochim. Biophys. Acta 1800*, 487-510.

(2) Peterson, T. E., and Manning, H. C. (2009) Molecular imaging: ^{18}F-FDG PET and a whole lot more. *J. Nucl. Med. Tech. 37*, 151-161.

(3) Mankoff, D. A. (2007) A definition of molecular imaging. *J Nucl Med 48*, 18N.

(4) Rahmim, A., and Zaidi, H. (2008) PET versus SPECT: Strengths, limitations and challenges. *Nucl. Med. Commun. 29*, 193-207.

(5) Schlyer, D. J. (2003) Chapter 1 Production of Radionuclides in Accelerators, in *Handbook of Radiopharmaceuticals: Radiochemistry and Applications* (Welch, M. J., Redvanly C. S., Ed.), Wiley, New York.

(6) Sonzogni, A. NuDat 2.4. National Nuclear Data Center (NNDC), Brookhaven National Laboratory, Accessed August 2011, http://www.nndc.bnl.gov/nudat2/.

(7) Vallee, B. L., and Falchuk, K. H. (1993) The biochemical basis of zinc physiology. *Physiol. Rev. 73*, 79-118.

(8) (2004 - 2012) Molecular Imaging and Contrast Agent Database (MICAD). Bethesda (MD): National Center for Biotechnology Information (US), Accessed November 8th 2012, http://www.ncbi.nlm.nih.gov/books/NBK5330/.

(9) Antunes, P., Ginj, M., Zhang, H., Waser, B., Baum, R. P., Reubi, J. C., and Maecke, H. (2007) Are radiogallium-labelled DOTA-conjugated somatostatin analogues superior to those labelled with other radiometals? *Eur. J. Nucl. Med. Mol. Imaging 34*, 982-993.

(10) Breeman, W. A. P., De Jong, M., De Blois, E., Bernard, B. F., Konijnenberg, M., and Krenning, E. P. (2005) Radiolabelling DOTA-peptides with ^{68}Ga. *Eur. J. Nucl. Med. Mol. Imaging 32*, 478-485.

(11) Liu, S. (2009) Radiolabeled cyclic RGD peptides as integrin $\alpha_v\beta_3$-targeted radiotracers: Maximizing binding affinity via bivalency. *Bioconjugate Chem. 20*, 2199-2213.

(12) André, J. P., Maecke, H. R., Zehnder, M., Macko, L., and Akyel, K. G. (1998) 1,4,7-Triazacyclononane-1-succinic acid-4,7-diacetic acid (NODASA): A new bifunctional chelator for radio gallium-labelling of biomolecules. *Chem. Commun.*, 1301-1302.

(13) Jae, M. J., Mee, K. H., Young, S. C., Lee, Y. S., Young, J. K., Gi, J. C., Dong, S. L., Chung, J. K., and Myung, C. L. (2008) Preparation of a promising angiogenesis PET imaging agent: ^{68}Ga-labeled c(RGDyK)-isothiocyanatobenzyl-1,4,7-triazacyclononane-1,4,7-triacetic acid and feasibility studies in mice. *J. Nucl. Med. 49*, 830-836.

(14) Riss, P. J., Kroll, C., Nagel, V., and Rösch, F. (2008) NODAPA-OH and NODAPA-$(NCS)_n$: Synthesis, ^{68}Ga-radiolabelling and in vitro characterisation of novel versatile bifunctional chelators for molecular imaging. *Bioorg. Med. Chem. Lett. 18*, 5364-5367.

(15) Eisenwiener, K. P., Prata, M. I. M., Buschmann, I., Zhang, H. W., Santos, A. C., Wenger, S., Reubi, J. C., and Mäcke, H. R. (2002) NODAGATOC, a new chelator-coupled somatostatin analogue labeled with [$^{67/68}$Ga] and [^{111}In] for SPECT, PET, and targeted therapeutic applications of somatostatin receptor (hsst2) expressing tumors. *Bioconjugate Chem. 13*, 530-541.

(16) Uehara, T., Guerra Gomez, F. L., Rokugawa, T., and Arano, Y. (2011) A new triazacyclononane-based ligand for trivalent ^{68}Ga tracers of high stability for positron emission tomography. *J. Nucl. Med. 52 (Supplement 1)*, 1473.

(17) Singh, A. N., Liu, W., Hao, G., Kumar, A., Gupta, A., Oz, O. K., Hsieh, J.-T., and Sun, X. (2011) Multivalent Bifunctional Chelator Scaffolds for Gallium-68 Based Positron Emission Tomography Imaging Probe Design: Signal Amplification via Multivalency. *Bioconjugate Chem. 22*, 1650-1662.

(18) Chen, X., Tohme, M., Park, R., Hou, Y., Bading, J. R., and Conti, P. S. (2004) Micro-PET imaging of $\alpha_v\beta_3$-integrin expression with^{18}F-labeled dimeric RGD peptide. *Mol. Imaging 3*, 96-104.

(19) Dijkgraaf, I., Yim, C.-B., Franssen, G., Schuit, R., Luurtsema, G., Liu, S., Oyen, W., and Boerman, O. (2011) PET imaging of $\alpha_v\beta_3$ integrin expression in tumours with ^{68}Ga-labelled mono-, di- and tetrameric RGD peptides. *Eur. J. Nucl. Med. Mol. Imaging 38*, 128-137.

(20) Li, Z. B., Chen, K., and Chen, X. (2008) ^{68}Ga-labeled multimeric RGD peptides for microPET imaging of integrin $\alpha_v\beta_3$ expression. *Eur. J. Nucl. Med. Mol. Imaging 35*, 1100-1108.

(21) Liu, S. (2006) Radiolabeled multimeric cyclic RGD peptides as integrin $\alpha_v\beta_3$ targeted radiotracers for tumor imaging. *Mol. Pharmaceutics 3*, 472-487.

(22) Devirgiliis, C., Zalewski, P. D., Perozzi, G., and Murgia, C. (2007) Zinc fluxes and zinc

transporter genes in chronic diseases. *Mutat. Res. 622*, 84-93.

(23) Lyster, D. M., and Noujaim, A. A. (1974) The unit dose preparation of ^{63}Zn-EDTA for use in Nuclear Medicine. *Int. J. Nucl. Med. Biol. 1*, 220-3.

(24) Fujibayashi, Y., Saji, H., Kawai, K., Unuma, Y., Miyata, S., Okuno, T., Hosotani, R., Inoue, K., Adachi, H., Horiuchi, K., and et al. (1986) A radiopharmaceutical for pancreatic exocrine functional diagnosis: ^{62}Zn-EDDA metabolism in pancreas. *Int. J. Nucl. Med. Biol. 12*, 447-51.

(25) Fujibayashi, Y., Saji, H., Yomoda, I., Kawai, K., Horiuchi, K., Adachi, H., Torizuka, K., and Yokoyama, A. (1986) ^{62}Zn-EDDA: a radiopharmaceutical for pancreatic functional diagnosis. *Int. J. Nucl. Med. Biol. 12*, 439-46.

(26) Fujibayashi, Y., Saji, H., Yomoda, I., Suzuki, K. H., Torizuka, K., and Yokoyama, A. (1986) A new approach toward a pancreas-seeking zinc radiopharmaceutical. II. ^{62}Zn-EDDA (ethylenediamine-N,N'-diacetic acid) for pancreas PCT imaging. *Eur. J. Nucl. Med. 11*, 488-93.

(27) Fujibayashi, Y., Saji, H., Yomoda, I., Suzuki, K. H., Torizuka, K., and Yokoyama, A. (1986) A new approach toward a pancreas-seeking zinc radiopharmaceutical. I. Accumulation of ^{65}Zn-amino acid and aminopolycarboxylic acid complexes in pancreatic tissue slices. *Eur. J. Nucl. Med. 11*, 484-7.

(28) Jalilian, A. R., Rowshanfarzad, P., Rahiminejad-Kisomi, A., Moradkhani, S., and Motamedi-Sedeh, F. (2004) Preparation, Biodistribution and Stability of [^{65}Zn] Bleomycin Complex. *DARU 12*, 115-22.

(29) Neirinckx, R. D. (1977) Excitation function for the ^{60}Ni (α,2n) ^{62}Zn reaction and production of ^{62}Zn bleomycin. *Int. J. Appl. Radiat. Isot. 28*, 808-809.

(30) Takeda, A. (2000) Movement of zinc and its functional significance in the brain. *Brain Res. Rev. 34*, 137-148.

(31) Takeda, A. (2004) Analysis of brain function and prevention of brain diseases: The action of trace metals. *Journal of Health Science 50*, 429-442.

(32) Takeda, A., Tamano, H., Enomoto, S., and Oku, N. (2001) Zinc-65 imaging of rat brain tumors. *Cancer Res. 61*, 5065-9.

(33) Takeda, A., Tamano, H., and Oku, N. (2003) Alteration of zinc concentrations in the brain implanted with C6 glioma. *Brain Res. 965*, 170-3.

(34) Tamano, H., Enomoto, S., Oku, N., and Takeda, A. (2002) Preferential uptake of zinc, manganese, and rubidium in rat brain tumor. *Nucl. Med. Biol. 29*, 505-508.

(35) F. Tárkányi, S. T., K. Gul, A. Hermanne, M. G. Mustafa, M. Nortier, P. Obložinský, S. M. Qaim, B. Scholten, N Yu. Shubin, Zhuang Youxiang. (2007) pp 77-93, IAEA.

(36) Tanaka, S. (1960) Reactions of nickel with alpha-particles. *J. Phys. Soc. Jpn. 15*, 2159-2167.

(37) Ziegler, J. F. (2008) Software SRIM.exe. Ver. 2008-03.

(38) H. H. Andersen, J. F. Z. (1977) *Hydrogen Stopping Powers and Ranges in all Elements*, Vol. 3, Pergamon Press, Oxford.

(39) H. Piel, S. M. Q., G. Stoecklin. (1992) Excitation functions of (p,xn)-Reactions on ^{nat}Ni and Highly Enriched ^{62}Ni: Possibility of Production of Medically Important Radioisotope ^{62}Cu at a small Cyclotron. *Radiochim. Acta 57*.

(40) Fukumura, T., Okada, K., Suzuki, H., Nakao, R., Mukai, K., Szelecsényi, F., Kovács, Z., and Suzuki, K. (2006) An improved ^{62}Zn/^{62}Cu generator based on a cation exchanger and its fully remote-controlled preparation for clinical use. *Nucl. Med. Biol. 33*, 821-827.

(41) Visser, E. P., Disselhorst, J. A., Brom, M., Laverman, P., Gotthardt, M., Oyen, W. J., and Boerman, O. C. (2009) Spatial resolution and sensitivity of the Inveon small-animal PET scanner. *J. Nucl. Med. 50*, 139-47.

(42) Strelow, F. W. E., Victor, A. H., Van Zyl, C. R., and Eloff, C. (1971) Distribution coefficients and cation exchange behavior of elements in hydrochloric acid-acetone. *Anal. Chem. 43*, 870-876.

(43) Yano, Y., and Budinger, T. F. (1977) Cyclotron produced Zn 62: Its possible use in prostate and pancreas scanning as a Zn 62 amino acid chelate. *J. Nucl. Med. 18*, 815-821.

(44) Sheline, G. E., Chaikoff, I. L., Jones, H. B., and Montgomery, M. L. (1943) STUDIES ON THE METABOLISM OF ZINC WITH THE AID OF ITS RADIOACTIVE ISOTOPE. *J. Biol. Chem. 147*, 409-414.

(45) Sheline, G. E., Chaikoff, I. L., Jones, H. B., and Montgomery, M. L. (1943) STUDIES ON THE METABOLISM OF ZINC WITH THE AID OF ITS RADIOACTIVE ISOTOPE. *J. Biol. Chem. 149*, 139-151.

(46) Dodson, G., and Steiner, D. (1998) The role of assembly in insulin's biosynthesis. *Curr. Opin. Struct. Biol. 8*, 189-194.

(47) Emdin, S. O., Dodson, G. G., Cutfield, J. M., and Cutfield, S. M. (1980) Role of zinc in insulin biosynthesis. Some possible zinc-insulin interactions in the pancreatic B-cell. *Diabetologia 19*, 174-182.

(48) Dunn, M. F. (2005) Zinc-ligand interactions modulate assembly and stability of the insulin hexamer - A review. *BioMetals 18*, 295-303.

(49) Chimienti, F., Devergnas, S., Favier, A., and Seve, M. (2004) Identification and cloning of a beta-cell-specific zinc transporter, ZnT-8, localized into insulin secretory granules. *Diabetes 53*, 2330-7.

(50) Chimienti, F., Favier, A., and Seve, M. (2005) ZnT-8, a pancreatic beta-cell-specific zinc transporter. *Biometals 18*, 313-7.

(51) Saudek, F., Brogren, C. H., and Manohar, S. (2008) Imaging the Beta-cell mass: why and how. *Rev. Diabet. Stud. 5*, 6-12.

(52) Greenlaw, R. H., Strain, W. H., Callear, T. E., Dubilier, L. D., and Strain, S. C. (1962) Experimental studies for scintillation scanning of the pancreas. *J. Nucl. Med. 3*, 47-50.

(53) Atkins, H. L., and Yano, Y. (1979) Pancreas uptake of zinc thioglucose. *Int J Nucl Med Biol 6*, 54-57.

(54) Fani, M., André, J. P., and Maecke, H. R. (2008) ^{68}Ga-PET: a powerful generator-based alternative to cyclotron-based PET radiopharmaceuticals. *Contrast Media Mol. Imaging 3*, 67-77.

(55) Clarke, E. T., and Martell, A. E. (1991) Stabilities of the Fe(III), Ga(III) and In(III) chelates of N,N′,N″-triazacyclononanetriacetic acid. *Inorg. Chim. Acta 181*, 273-280.

(56) Ferreira, C. L., Lamsa, E., Woods, M., Duan, Y., Fernando, P., Bensimon, C., Kordos, M., Guenther, K., Jurek, P., and Kiefer, G. E. (2010) Evaluation of bifunctional chelates for the development of gallium-based radiopharmaceuticals. *Bioconjugate Chem. 21*, 531-536.

(57) Velikyan, I., Maecke, H., and Langstrom, B. (2008) Convenient preparation of ^{68}Ga-based PET-radiopharmaceuticals at room temperature. *Bioconjugate Chem. 19*, 569-573.

(58) Notni, J., Hermann, P., Havlíčková, J., Kotek, J., Kubíček, V., Plutnar, J., Loktionova,

N., Riss, P. J., Rösch, F., and Lukeš, I. (2010) A triazacyclononane-based bifunctional phosphinate ligand for the preparation of multimeric ^{68}Ga tracers for positron emission tomography. *Chem. Eur. J. 16*, 7174-7185.

(59) Notni, J., Šimeček, J., Hermann, P., and Wester, H. J. (2011) TRAP, a powerful and versatile framework for gallium-68 radiopharmaceuticals. *Chem. Eur. J. 17*, 14718-14722.

(60) Abiraj, K., Jaccard, H., Kretzschmar, M., Helm, L., and Maecke, H. R. (2008) Novel DOTA-based prochelator for divalent peptide vectorization: Synthesis of dimeric bombesin analogues for multimodality tumor imaging and therapy. *Chem. Commun.*, 3248-3250.

(61) Woods, M., Aime, S., Botta, M., Howard, J. A. K., Moloney, J. M., Navet, M., Parker, D., Port, M., and Rousseaux, O. (2000) Correlation of Water Exchange Rate with Isomeric Composition in Diastereoisomeric Gadolinium Complexes of Tetra(carboxyethyl)dota and Related Macrocyclic Ligands. *J. Am. Chem. Soc. 122*, 9781-9792.

(62) Šimeček, J., Schulz, M., Notni, J., Plutnar, J., Kubíček, V., Havlíčková, J., and Hermann, P. (2012) Complexation of metal ions with TRAP (1,4,7-triazacyclononane phosphinic acid) ligands and 1,4,7-triazacyclononane-1,4,7-triacetic acid: Phosphinate-containing ligands as unique chelators for trivalent gallium. *Inorg. Chem. 51*, 577-590.

(63) Cantorias, M. V., Howell, R. C., Todaro, L., Cyr, J. E., Berndorff, D., Rogers, R. D., and Francesconi, L. C. (2007) MO Tripeptide Diastereomers (M = $^{99/99m}$Tc, Re): Models To Identify the Structure of ^{99m}Tc Peptide Targeted Radiopharmaceuticals. *Inorg. Chem. 46*, 7326-7340.

(64) Cyr, J. E., Pearson, D. A., Nelson, C. A., Lyons, B. A., Zheng, Y., Bartis, J., He, J., Cantorias, M. V., Howell, R. C., and Francesconi, L. C. (2007) Isolation, Characterization, and Biological Evaluation of Syn and Anti Diastereomers of [^{99m}Tc]Technetium Depreotide: a Somatostatin Receptor Binding Tumor Imaging Agent. *J. Med. Chem. 50*, 4295-4303.

(65) Haubner, R., Wester, H. J., Reuning, U., Senekowitsch-Schmidtke, R., Diefenbach, B., Kessler, H., Stöcklin, G., and Schwaiger, M. (1999) Radiolabeled $\alpha_v\beta_3$ integrin antagonists: A new class of tracers for tumor targeting. *J. Nucl. Med. 40*, 1061-1071.

(66) Eisenwiener, K. P., Powell, P., and Mäcke, H. R. (2000) A convenient synthesis of

novel bifunctional prochelators for coupling to bioactive peptides for radiometal labelling. *Bioorg. Med. Chem. Lett. 10*, 2133-2135.

(67) Imai, S., Morimoto, J., Tsubura, Y., Esaki, K., Michalides, R., Holmes, R. S., von Deimling, O., and Hilgers, J. (1986) Genetic marker patterns and endogenous mammary tumor virus genes in inbred mouse strains of Japan. *Exp. anim. 35*, 263-273.

(68) Pierrard, J. C., Rimbault, J., Aplincourt, M., Le Greneur, S., and Port, M. (2008) New synthesis of a high molecular weight ligand derived from dota; thermodynamic stability of the MRI contrast agent formed with gadolinium. *Contrast Media Mol. Imaging 3*, 243-252.

(69) Jia, B., Liu, Z., Shi, J., Yu, Z., Yang, Z., Zhao, H., He, Z., Liu, S., and Wang, F. (2008) Linker effects on biological properties of ^{111}In-labeled DTPA conjugates of a cyclic RGDfK dimer. *Bioconjugate Chem. 19*, 201-210.

(70) Chen, X., Park, R., Shahinian, A. H., Bading, J. R., and Conti, P. S. (2004) Pharmacokinetics and tumor retention of ^{125}I-labeled RGD peptide are improved by PEGylation. *Nucl. Med. Biol. 31*, 11-19.

(71) Souers, A. J., Schürer, S., Kwack, H., Virgilio, A. A., and Ellman, J. A. (1999) Preparation of enantioenriched α-bromo acids incorporating diverse functionality. *Synthesis*, 583-585.

(72) Geysen, H. M. (2007) Methods and Materials for Preparing Organic Compounds from Primary Amines. WO 2007/117404. WIPO-Patent Cooperation Treaty (PCT)

(73) Moore, D. A., Fanwick, P. E., and Welch, M. J. (1990) A novel hexachelating amino-thiol ligand and its complex with gallium(III). *Inorg. Chem. 29*, 672-676.

(74) Bandoli, G., Dolmella, A., Tisato, F., Porchia, M., and Refosco, F. (2009) Mononuclear six-coordinated Ga(III) complexes: A comprehensive survey. *Coord. Chem. Rev. 253*, 56-77.

(75) Knetsch, P. A., Petrik, M., Griessinger, C. M., Rangger, C., Fani, M., Kesenheimer, C., Von Guggenberg, E., Pichler, B. J., Virgolini, I., Decristoforo, C., and Haubner, R. (2011) NODAGA-RGD for imaging $\alpha_v\beta_3$ integrin expression. *Eur. J. Nucl. Med. Mol. Imaging 38*, 1303-1312.

(76) Morfin, J. F., and Tóth, E. (2011) Kinetics of Ga(NOTA) formation from weak Ga-citrate complexes. *Inorg. Chem. 50*, 10371-10378.

(77) Brucher, E., and Sherry, A. D. (1990) Kinetics of formation and dissociation of the 1,4,7-triazacyclonononane-N,N',N''-triacetate complexes of cerium(III), gadolinium(III), and erbium(III) ions. *Inorganic Chem. 29*, 1555-1559.

(78) Chang, C. A., Liu, Y. L., Chen, C. Y., and Chou, X. M. (2001) Ligand preorganization in metal ion complexation: Molecular mechanics/dynamics, kinetics, and laser-excited luminescence studies of trivalent lanthanide complex formation with macrocyclic ligands TETA and DOTA. *Inorg. Chem. 40*, 3448-3455.

(79) Moreau, J., Guillon, E., Pierrard, J. C., Rimbault, J., Port, M., and Aplincourt, M. (2004) Complexing mechanism of the lanthanide cations Eu^{3+}, Gd^{3+}, and Tb^{3+} with 1,4,7,10-tetrakis (carboxymethyl)-1,4,7, 10-tetraazacyclododecane (dota) - characterization of three successive complexing phases: Study of the thermodynamic and structural properties of the complexes by potentiometry, luminescence spectroscopy, and EXAFS. *Chem. Eur. J. 10*, 5218-5232.

(80) Wang, L., Shi, J., Kim, Y.-S., Zhai, S., Jia, B., Zhao, H., Liu, Z., Wang, F., Chen, X., and Liu, S. (2008) Improving Tumor-Targeting Capability and Pharmacokinetics of ^{99m}Tc-Labeled Cyclic RGD Dimers with PEG_4 Linkers. *Mol. Pharmaceutics 6*, 231-245.

(81) Liu, Z., Niu, G., Shi, J., Liu, S., Wang, F., and Chen, X. (2009) ^{68}Ga-labeled cyclic RGD dimers with Gly_3 and PEG_4 linkers: Promising agents for tumor integrin $\alpha_v\beta_3$ PET imaging. *Eur. J. Nucl. Med. Mol. Imaging 36*, 947-957.

(82) Li, Z. B., Cai, W., Cao, Q., Chen, K., Wu, Z., He, L., and Chen, X. (2007) ^{64}Cu-labeled tetrameric and octameric RGD peptides for small-animal PET of tumor $\alpha_v\beta_3$ integrin expression. *J. Nucl. Med. 48*, 1162-1171.

(83) Garanger, E., Boturyn, D., Coll, J.-L., Favrot, M.-C., and Dumy, P. (2006) Multivalent RGD synthetic peptides as potent $\alpha_v\beta_3$ integrin ligands. *Org. Biomol. Chem. 4*, 1958-1965.

(84) Wu, Y., Zhang, X., Xiong, Z., Cheng, Z., Fisher, D. R., Liu, S., Gambhir, S. S., and Chen, X. (2005) microPET imaging of glioma integrin $\alpha_v\beta_3$ expression using ^{64}Cu-labeled tetrameric RGD peptide. *J. Nucl. Med. 46*, 1707-1718.

(85) Wu, Z., Li, Z.-B., Chen, K., Cai, W., He, L., Chin, F. T., Li, F., and Chen, X. (2007) microPET of Tumor Integrin $\alpha_v\beta_3$ Expression Using ^{18}F-Labeled PEGylated Tetrameric RGD Peptide (^{18}F-FPRGD4). *J. Nucl. Med. 48*, 1536-1544.

(86) Akizawa, H., Uehara, T., and Arano, Y. (2008) Renal uptake and metabolism of

radiopharmaceuticals derived from peptides and proteins. *Adv. Drug Deliv. Rev. 60*, 1319-1328.

(87) Loktionova, N. S., Belozub, A. N., Filosofov, D. V., Zhernosekov, K. P., Wagner, T., Türler, A., and Rösch, F. (2011) Improved column-based radiochemical processing of the generator produced ^{68}Ga. *Appl. Radiat. Isot. 69*, 942-946.

(88) Dumont, R. A., Deininger, F., Haubner, R., Maecke, H. R., Weber, W. A., and Fani, M. (2011) Novel ^{64}Cu- and ^{68}Ga-labeled RGD conjugates show improved PET imaging of $\alpha_v\beta_3$ integrin expression and facile radiosynthesis. *J. Nucl. Med. 52*, 1276-1284.

Associated articles

Francisco L. Guerra Gómez, Yuuki Takada, Rie Hosoi, Sotaro Momosaki, Kazuhiko Yanamoto, Kotaro Nagatsu, Hisashi Suzuki, Ming-Rong Zhang, Osamu Inoue, Yasushi Arano, Toshimitsu Fukumura: Production and purification of the positron emitter zinc-63. J. Label Compd. Radiopharm. 55(1), 5–9 (2012)

Francisco L. Guerra Gomez, Tomoya Uehara, Takemi Rokugawa, Yusuke Higaki, Hiroyuki Suzuki, Hirofumi Hanaoka, Hiromichi Akizawa, and Yasushi Arano: Synthesis and evaluation of diastereoisomers of 1,4,7-triazacyclononane-1,4,7-tris-(glutaric acid) (NOTGA) for multimeric radiopharmaceuticals of gallium. Bioconjugate Chem. 23(11), 2229–2238 (2012)

Dissertation committee

This dissertation was evaluated by the following committee authorized by the Graduate School of Medical and Pharmaceutical Sciences of Chiba University:

Chief Examiner:

Prof. Toida Toshihiko, PhD. Clinical and Analytical Biochemistry Department

Associate examiners:

Prof. Neya Saburo, PhD. Physical Chemistry Department

Prof. Nishida Atsushi, PhD. Synthetic Organic Chemistry Department

All affiliated to the Graduate School of Medical and Pharmaceutical Sciences of Chiba University

Acknowledgements

I would like to thank in first place to my academic advisor Prof. Arano Yasushi for getting me into to the world of Pharmacology and successfully guiding me until the end after 7 years of studies. Without his encourage in would have been impossible the realization of the present work. Assoc. Prof Uehara Tomoya is also an indispensable person in my work, and a source of extraordinary and kind support as a teacher and as a friend. Thank to Assoc. Prof. Hanaoka Hirofumi for lecturing me how to face not only science but life.

Thanks to the dissertation committee: Prof. Toida Toshihiko, Prof. Neya Saburo and Prof. Nishida Atsushi.

The members of the Department of Molecular Imaging and Radiotherapy of the Medical and Pharmaceutical Sciences Faculty of the University of Chiba share with me friendship and youth; thank especially to Rokugawa Takemi, from who I borrowed invaluable knowledge, Yanagi Mashiho for her unconditional support; Khajadpai Thipyapong for his advices, Hiroyuki Suzuki for his collaboration, Higaki Yuusuke for his SPECT/CT images, Mrs. Nagai always ready to help on whatever we need and the late Prof. Taira. Prof. Suzuki Noriyuki and Prof. Kagawa for their support in the NMR measurements.

Along with my professors, all of them members of the Pharmacy Faculty Office, and Mrs. Shibuya and Mrs. Kaori from the International Support Desk supported me in the twist and turns of my international affairs. Thank you very much.

Thanks to the National Center of Radiological Sciences of Japan that influenced deeply to my formation from the office staff, researchers all to the operation staff of the cyclotrons. Especially, to my mentor PhD. Fukumura Toshimitsu who also guided me to the realization of

the present dissertation. The colleagues of the Moleculat Probe Group, PhD. Nagatsu Kootaro, who always supported me, Mr. Takeda, another source of knowledge, Mr. Suzuki H., Mr. Fukada and Mr. Mineguishi, without them I would have not made my path through the irradiation room labyrinth.

Thank to people like Prof. Tatsuo Ido, Prof. Suzuki K., Prof. Honma, Prof. Inoue and Prof. Zhang for they disinterested help; extensive also to my colleagues in the papers.

Special thanks to the members of the National Center of Nuclear Safety of Cuba and the directors Mr.Ulises, Mrs Aniuska and Mrs Alba who backed my life decisions. To my friends there: my eternal gratitude.

I gratefully acknowledge the funding sources that made my Ph.D. possible; The Ministry of Science Culture and Sport of Japan (MEXT) for the 6 years of Monbukagakusho Scholarship and the Yamada Osamitsu Scholarship Foundation that made me the opportunity to make valuable friends in the last year. The work was also partially supported by Special Funds for Education and Research from MEXT and FUJIFILM RI Pharma Co., Ltd. provided the $[^{67}Ga]Cl_3$ that made my experiments possible.

These years in Japan have been wonderful thank greatly to close friends that have been there through thick and thin.

Lastly, I would like to thank my family for their love and support. To my mother who taught me the love for studying, my brothers and sisters, and their kids that has been always a source of inspiration. Thank you.

Francisco Lázaro Guerra Gómez
Chiba University
2012